# A panel of KSHV mutants in the polycistronic kaposin locus for precise analysis of individual protein products

Mariel Kleer[1,2,3], Grant MacNeil[4], Eric S. Pringle[4], and Jennifer A. Corcoran[1,2,3,4 #]

[1] Microbiology, Immunology and Infectious Diseases Department, University of Calgary, Calgary, AB, Canada.

[2]Charbonneau Cancer Institute, University of Calgary, Calgary, AB, Canada.

[3]Snyder Institute for Chronic Diseases, University of Calgary, Calgary, AB, Canada.

[4]Department of Microbiology and Immunology, Dalhousie University, Halifax, NS, Canada

[#]Corresponding Author

## Abstract

Kaposi's sarcoma-associated herpesvirus (KSHV) is the infectious cause of several human cancers including the endothelial cell (EC) malignancy, Kaposi's sarcoma. Unique KSHV genes absent from other human herpesvirus genomes, known as "K-genes", are typically important for KSHV replication and pathogenesis. Among the K-genes, the kaposin mRNA is highly expressed in both latent and lytic phases of infection, but its polycistronic nature has hindered methodical analysis of the role of kaposin translation products in viral replication. At least three proteins are produced from the kaposin transcript, Kaposin A (KapA), B (KapB), and C (KapC). We have previously shown that KapB overexpression is sufficient to recapitulate two KS phenotypes, EC spindling and elevated proinflammatory cytokine transcripts, the latter which proceeds via the disassembly of RNA decay granules called processing bodies (PBs). To pinpoint the relative contributions of kaposin proteins at different stages of KSHV infection, we constructed four recombinant viruses by deleting or recoding the *kaposin* locus. Latent infection of iSLK cells with kaposin-deficient viruses resulted in reduced viral genome copy number and small LANA nuclear bodies; despite this, all iSLK cells were capable of progeny virion production. *De novo* infection of ECs revealed that KapB was dispensable for EC spindling but required for PB disassembly during KSHV latency, suggesting other viral proteins contribute to spindling. These findings demonstrate that our panel of viruses enables precise analysis of respective contributions of individual kaposin proteins to KSHV replication. This approach serves as a guide for the functional analysis of complex multicistronic viral loci.

## Importance

Kaposi's sarcoma-associated herpesvirus (KSHV) expresses high levels of the kaposin transcript during both latent and lytic phases of replication. Due to its repetitive, GC-rich nature and

polycistronic coding capacity, until now no reagents existed to permit a methodical analysis of the role of individual kaposin proteins in KSHV replication. We report the creation of a panel of recombinant viruses and matched producer cell lines that delete kaposin proteins individually or in combination. We demonstrate the utility of this panel by confirming the requirement of one kaposin translation product to a key KSHV latency phenotype. This study describes a new panel of molecular tools for the KSHV field to enable precise analysis of the roles of individual kaposin proteins during KSHV infection.

## Introduction

Kaposi's sarcoma-associated herpesvirus (KSHV) is the infectious cause of the endothelial cell (EC) neoplasm, Kaposi's sarcoma (KS) and two rare lymphoproliferative disorders: primary effusion lymphoma (PEL) and multicentric Castleman disease (MCD) (1–3). Like all herpesviruses, KSHV establishes persistent, life-long infection of its human host, and displays two modes of infection, latent and lytic replication. Latency is the default replication program upon *de novo* infection in most cell types (4, 5). Following a transient period of lytic gene expression which serves to amplify genome copy number and evade the intrinsic immune response (6, 7), the viral episome is circularized and tethered to the host chromosome by the viral latency-associated nuclear antigen (LANA) (8). This results in formation of microscopically visible LANA-nuclear bodies (NB), which correlate with intracellular viral genome copy number (9–13). In the latent state, the viral genome is passively replicated and unevenly partitioned to daughter cells by host cell machinery (10, 14, 15). The viral genome will remain in a highly chromatinized state until expression of the viral lytic switch protein, replication and transcription activator (RTA), which is both necessary and sufficient for lytic reactivation (16–18). Following reactivation, lytic gene expression follows a prescribed temporal cascade with genome replication marking the transition from early to late gene expression (19, 20). More recent analyses using single cell approaches describe lytic induction as a heterogenous population of infected cells that display various stages of reactivation (13, 21–23). The lytic replication phase produces progeny virions enabling transmission of the virus and culminates in cell death.

The KSHV-infected cells in KS lesions are predominantly proliferating endothelial cells (ECs) with an abnormal elongated or 'spindled' morphology. The majority of these tumor ECs exhibit latent KSHV infection, whereas lytic replication is limited (24–27). Lytic replication is

67 hypothesized to play a role in KS, likely due to the ongoing production of progeny virions as
68 well as the release of inflammatory and angiogenic factors (14, 28, 29). Consistent with this,
69 limiting viral lytic replication caused KS regression, suggesting that spontaneous lytic
70 reactivation is required for ongoing infection of naïve cells in the tumor environment and
71 supports the cancer (30–32).

72 As latently infected cells comprise the bulk of the KS lesion, the contribution of KSHV
73 latent gene expression to tumorigenesis has been explored extensively in both animal and cell
74 culture models (29, 33–37). *In vitro* infection of primary ECs with KSHV recapitulates many of
75 the features of KS tumors, including efficient establishment of viral latency. During latency,
76 gene expression is limited to six consensus protein products produced from an approximately
77 10kbp region of the viral genome termed the latency locus (LANA, viral cyclin [v-Cyclin], and
78 viral fas-associated death domain (FADD)-like interleukin-1-β-converting enzyme (FLICE)
79 inhibitory protein [v-FLIP], Kaposins [Kap] A, B, and C) and 12 pre-miRNAs that are processed
80 into at least 25 mature miRNAs (38–41) Using ectopic expression models, several latent gene
81 products have been shown to contribute to the establishment and maintenance of viral latency as
82 well as phenotypes associated with KS tumors (reviewed in (42, 43), but these studies have
83 predominantly focused on LANA, v-Cyclin and v-FLIP while the contributions of the
84 polycistronic kaposin locus is less clear. The kaposin mRNA was first identified as a marker of
85 KSHV latent infection in KS tumours in 1997 (27), and it remains the dominant viral transcript
86 in KS tumor isolates (44). The kaposin locus comprises a significant fraction of KSHV coding
87 capacity during latency and kaposin transcription is also upregulated during lytic replication,
88 suggesting that this region of the viral genome is important (45). Despite this, we still know very
89 little about the role of the kaposin locus, or the proteins it encodes, during viral replication.

90 The kaposin transcript is polycistronic and can be translated into at least three
91 polypeptides, KapA, KapB and KapC (Figure 1A) (45), though we and others have observed
92 multiple banding patterns on immunoblots that suggest additional translation products may also
93 be derived from this locus (45, 46). Translation of KapA is initiated at a canonical AUG start
94 codon located distal to the 5' end of the transcript and encodes a small membrane spanning
95 protein (47–49). KapC is translated in the same reading frame as KapA, making its carboxy-
96 terminal region identical to KapA. However, translation of KapC is initiated at one of two
97 possible non-canonical CUG start codons proximal to the 5' end of the transcript. Therefore, in
98 addition to the KapA ORF, the KapC translation product contains two 23-amino acid direct
99 repeat (DR) regions termed DR1 and DR2 (DR1: PSSPGTWCPPPREPGALLPGNLV and DR2:
100 APQEPGAAHPRNPARRTPGTRRG) which are derived from three sets of GC-rich 23-
101 nucleotide repeats (Figure 1A-B). Translation of KapB is initiated at one of two possible non-
102 canonical CUG or GUG start codons that are most proximal to the 5' end of the kaposin mRNA,
103 but uses an alternative reading frame to that of KapA/C. The resulting polypeptide is comprised
104 largely of the same two 23-amino acid DRs (DR1 and DR2) found in KapC (Figure 1B) but
105 lacks the C-terminal membrane spanning domain found in both KapA and KapC. Moreover,
106 different isolates of KSHV display expansion or contraction of both direct repeats, the functional
107 significance of which is unknown, yet regardless of the diversity in size, the core DR1 and DR2
108 repeats remain constant (45).

109 Our knowledge about individual kaposin protein function is derived largely from ectopic
110 expression of individual kaposin proteins. KapA was reported to promote cell transformation *in*
111 *vitro* and *in vivo* (47, 48); however, more recent work showed that this function stems from one
112 of the viral miRNAs embedded within the KapA ORF (50). Previous work from our group has

113 shown that KapB is sufficient to induce angiogenesis in an *in vitro* EC tubule formation assay
114 and to promote actin stress fibers and elongation of ECs into a spindled morphology that
115 recapitulates the morphology of latently infected KS tumor cells (51). KapB also is sufficient to
116 induce the disassembly of RNA granules called processing bodies (PBs) (51, 52). PBs are
117 important sites for the constitutive turnover or translational suppression of inflammatory
118 cytokine mRNAs; PB loss correlates with enhanced levels of inflammatory cytokine transcripts
119 that are normally targeted to PBs via an AU-rich destabilizing element (51, 53–57). However,
120 our previous studies could not determine if KapB alone is necessary for these phenotypes during
121 KSHV latent infection as we used RNA silencing to knockdown the kaposin transcript, a strategy
122 that reduced expression of all kaposin proteins (51). No other studies have determined the role of
123 individual kaposin translation products in KSHV latent or lytic replication cycles.

124 Here, we describe our use of the KSHV BAC16 bacterial artificial chromosome (BAC)
125 and lambda Red recombination system (58) to construct a panel virus defective for specific
126 *kaposin* locus products. We have constructed a triple deletion BAC16ΔKapABC, a double
127 deletion BAC16ΔKapBC, two single deletions BAC16ΔKapB and BAC16ΔKapC, and a partial
128 revertant into which we have re-inserted a single copy of both DR1 and DR2, called 1X DRs
129 (Figure 1C). We confirmed that these viruses no longer express the deleted kaposin-derived
130 proteins and show that all kaposin-deficient viruses are competent for genome replication and
131 production of progeny virions. However, we show that ΔKapB is significantly impaired, and
132 demonstrates markedly reduced genome copy number, small LANA nuclear bodies, and lower
133 LANA protein levels. Additionally, ΔKapB fails to cause PB disassembly following *de novo*
134 infection of primary ECs, showing for the first time that KapB is necessary for PB disassembly
135 during KSHV latency. With this panel of kaposin recombinant KSHV viruses, it is now feasible

136 to interrogate, with unprecedented precision, the role of individual kaposin protein products in

137 the context of KSHV latent or lytic infection.

138 **Materials and Methods:**

139 **Cell culture**

140 All cells were grown at 37°C with 5% $CO_2$ and atmospheric $O_2$. HEK293T cells (ATCC) were
141 cultured in DMEM (Thermo Fisher) supplemented with 100 U/mL penicillin, 100 µg/mL
142 streptomycin, 2 mM L-glutamine (Thermo Fisher) and 10% fetal bovine serum (FBS; Thermo
143 Fisher). iSLK.RTA cells (59) were cultured likewise with the addition of 1 µg/mL puromycin
144 and 250 µg/mL geneticin (Thermo Fisher). BAC16-iSLK.RTA cells were cultured similar to
145 iSLK.RTA cells, with the addition of 1200 µg/mL hygromycin B (Thermo Fisher). Human
146 umbilical vein endothelial cells (HUVECs, Lonza) were cultured in endothelial cell growth
147 medium (EGM-2) (Lonza). HUVECs were seeded onto gelatin (0.1% w/v in PBS)-coated tissue
148 culture plates or glass coverslips.

149 **Lambda Red recombination for BAC16 mutagenesis**

150 All mutagenesis was carried out in the BAC16 background (58) supplied in the GS1783 strain of
151 *Escherichia coli (E.coli)* (A generous gift from Dr. Jae Jung). All restriction enzymes were
152 purchased from New England Biolabs (NEB) and all primers were purchased from Invitrogen.

153 A kanamycin resistance and levansucrase enzyme cassette (KanSacB) was amplified using
154 primers (Table 1) with 40bp overhanging sequences that correspond to the K12 sequence of the
155 *kaposin* locus in the BAC16 genome. These primers also allowed for the introduction of BamHI
156 and NotI restriction endonuclease sites. The resulting PCR product was then subcloned into
157 pcDNA3.1+ (Addgene) using BamHI and NotI restriction endonucleases (pcDNA3.1+-
158 KanSacB).

159 To create single deletions of KapB and KapC, two direct repeat (DR) region gene blocks were
160 synthesized (BioBasic) where the third nucleotide of each codon of DR1 and DR2 was altered to
161 insert premature stop codons and nonsynonymous mutations into one frame, while creating
162 synonymous mutations in the other. This allowed the primary amino acid sequence of either
163 KapB or KapC to be maintained while eliminating expression from the other ORF and vice
164 versa. Primers were used to amplify the gene block with 40bp overhanging sequences that: 1)
165 flank the gene block, 2) are homologous to the upstream and downstream regions of the DRs in
166 the BAC16 genome, and 3) introduce NheI and BamHI restriction sites. The resulting PCR
167 product was then subcloned into pcDNA3.1+-KanSacB (described above) using NheI and
168 BamHI restriction sites (pcDNA3.1+-geneblock-KanSacB).

169 Lambda Red recombination was conducted in the GS1783 *E.coli* strain, which expresses
170 the I-Sce enzyme and, in a temperature (42°C) dependent manner, the lambda Red recombinase
171 genes (beta, exo and gam). BAC16-GS1783 *E. coli* were cultured at 30°C in Lysogeny Broth
172 (LB) containing 30 $\mu$g/mL chloramphenicol (Sigma-Aldrich) until reaching an optical density
173 ($OD_{600}$) of 0.6-0.8. Cultures were incubated for 30 minutes at 42°C prior to pelleting at room
174 temperature at 3000 x *g* for 5 minutes. Bacterial pellets were resuspended in $ddH_20$ and pelleted
175 again at 3000 x *g* for 5 minutes. This step was repeated once more, following which bacterial
176 pellets were resuspended in 50 $\mu$L $ddH_20$ and placed on ice. Meanwhile, pcDNA3.1+-geneblock-
177 KanSacB was digested with NheI and NotI restriction endonucleases to generate a linear DNA
178 fragment for recombination. This was purified by 1% agarose gel electrophoresis and gel
179 extracted according to QIAquick gel extraction kit (QIAGEN) standard protocol. The purified
180 fragment was electroporated (2.5kV, 25$\mu$F BioRad Gene Pulser®II) into 50 $\mu$L of $ddH_2O$-washed
181 BAC16-GS1783 *E.coli*. Bacteria was recovered for 1 hour in 1 mL of LB media at 30°C, plated

182 onto LB agar plates containing 50 µg/mL kanamycin, and incubated at 30°C overnight (O/N).
183 Colonies were screened for successful recombination using colony PCR and two sets of
184 screening primers designed to assess insert size and orientation (Table 1).

185 Colonies that produced bands of the expected size with both primer sets were inoculated
186 into 1 ml of LB containing 1% arabinose (Sigma-Aldrich) for 1 hour at 30°C to induce I-Sce
187 expression to linearize the inserted KanSacB cassette. Bacteria were then incubated at 42°C for
188 30 minutes to induce recombinase gene expression and recovered for 1 hour at 30°C prior to
189 plating on LB agar plates containing 30 $\mu$g/mL chloramphenicol and 5% sucrose, which selects
190 for the loss of SacB that synthesizes a toxic compound in the presence of sucrose. Positive
191 colonies were replica-plated on LB agar plates containing 50 µg/mL kanamycin. Those colonies
192 that grew on both chloramphenicol and sucrose containing plates, and which were no longer
193 kanamycin resistant, were screened by colony PCR for having undergone the second
194 recombination to remove the KanSacB cassette and colony PCR products were verified by
195 Sanger sequencing using primers as listed (Table 1).

196 **Isolation of BACmid DNA**

197 BACmid DNA was isolated from GS1783 *E.coli* cultures of 5 mL of LB containing 30 $\mu$g/mL
198 chloramphenicol grown O/N at 30°C. Bacteria was pelleted at 3000 x *g* for 5 minutes, re-
199 suspended in buffer P1 containing RNaseA, lysed using alkaline lysis in buffer P2 and
200 neutralized with buffer N3 (All reagents from QIAprep kits, QIAGEN). Following addition of
201 buffer N3, lysates were placed on ice for 10 minutes prior to centrifugation at 17 000 x *g* for 10
202 minutes to pellet precipitate. 750 µL of supernatant was then mixed with 750 µL of 100%
203 isopropanol and placed on ice for 10 minutes prior to centrifugation at 17 000 x *g* for 10 minutes

204 to pellet DNA. Supernatants were removed and the DNA pellet was left to air dry before being
205 resuspended in 50 µL 10mM Tris-Cl, pH 8.5. DNA was used immediately for transfection.

206 **Whole genome sequencing of KSHV BACs**

207 BACmid DNA was isolated from GS1783 *E.coli* cultures of 400 mL LB containing 30 $\mu$g/mL
208 chloramphenicol grown O/N at 30°C. Bacteria was pelleted at 4000 x *g* for 10 minutes at 4˚C.
209 DNA was then extracted using the Qiagen Large Construct Kit in accordance with
210 manufacturer's protocol. Critically, this isolation includes an exonuclease step which removes
211 sheared *E.coli* DNA thereby allowing greater coverage of the BAC16 genome.

212 Whole genome sequencing was performed by the Centre for Health Genomics and
213 Informatics (University of Calgary, Calgary, AB). Briefly, libraries were prepared using a NEB
214 ultra II DNA Library Prep Kit for Illumina (NEB), quantified using a Kapa qPCR Library Kit
215 (Roche), and sequenced using a MiSeq 500 v2 nano run (MiSeq Reagent Kit v2, Illumina) to
216 generate 250+250bp paired end sequences. Raw reads were imported into Geneious Prime (60),
217 paired and trimmed according to default settings. Reads were then aligned to the BAC16
218 reference genome (NCBI accession #GQ994935). Average coverage was between ~670 and
219 1400x. Variations were identified based on a minimum coverage of 5 and minimum frequency in
220 variation of 0.25.

221 **Restriction length fragment polymorphism**

222 Isolated BACmid DNA was digested overnight using NheI restriction enzyme (New England
223 Biolabs) at 37°C. Digested DNA fragments were then subjected to 1% agarose pulsed-field gel
224 electrophoresis (PFGE) (Bio-Rad) using 0.5% Tris/Borate/EDTA (TBE) buffer and the following
225 conditions: 6 V/cm, 120° field angle, and switch time linearly ramped from 1 s to 5 s over 14-15

226 h (CHEF DR III, Bio-Rad). DNA bands were visualized by staining the gel with a solution of 0.5
227 µg/mL ethidium bromide; excess stain was washed away with deionized water and the gel was
228 imaged on a ChemiDoc Touch Imaging System (Bio-Rad). DNA molecular weight standard
229 (BioRad, CHEF DNA size 8-48-kb) was used as reference.

230 **Generation of Stable BAC16-iSLK.RTA cell lines**

231 6-well plates of 70% confluent 293T cells in antibiotic-free 10% FBS DMEM were washed once
232 with PBS, and media was replaced with 1 mL serum-free, antibiotic-free 10% FBS DMEM per
233 well prior to transfection. 5 uL of re-suspended DNA was incubated with 100 uL Opti-MEM
234 reduced serum media (Thermo Fisher) for 5 minutes. Separately, 18 uL of polyethylenimine
235 (PEI, Polysciences) was incubated with 100 uL Opti-MEM, also for 5 minutes. These two
236 mixtures were combined, incubated for 15 minutes, and added dropwise to each well. Cells were
237 incubated at 37°C for 4 hours at which time the media was replaced with antibiotic-free 10%
238 FBS DMEM before further incubation at 37C.

239 At 48 hours post transfection, cells were expanded into 10-cm dishes. One day later,
240 media was removed and replaced with fresh antibiotic-free 10% FBS DMEM containing 20
241 ug/mL hygromycin (Thermo Fisher Scientific). The concentration of hygromycin was steadily
242 increased until a final concentration of 100 $\mu$g/mL was reached. When a confluent monolayer of
243 hygromycin-resistant BAC16 293T cells was achieved, cells were split once prior to liquid N2
244 storage in 90% FBS and 10% dimethyl sulfoxide (DMSO, Sigma-Aldrich).

245 To generate latent iSLK cells, each population of BAC16-transfected 293T cells was
246 individually co-cultured with puromycin-resistant iSLK.RTA cells in a 6-well dish at a 2:1 ratio.
247 Once cells reached 80% confluency, media was replaced with antibiotic-free 10% FBS DMEM

248 containing 1 mM sodium butyrate (NaB, Sigma-Aldrich) and 20 ng/mL 12-O-
249 tetradecanoylphorbol-13-acetate (TPA, Sigma-Aldrich) to induce latent BAC16-293T cells to
250 produce progeny virions. At 96 hours post reactivation, cells were expanded into 10 cm dishes.
251 One day following expansion, media was replaced with antibiotic-free 10% FBS DMEM
252 containing 10 ug/mL puromycin and 100 $\mu$g/mL hygromycin. Hygromycin concentration was
253 steadily increased in approximately 50 $\mu$g/mL increments until a final concentration of 240
254 $\mu$g/mL was reached. Once a near-confluent monolayer of BAC16-iSLK.RTA cells was achieved,
255 cells were split once prior to liquid $N_2$ storage as above.

256 **Production of KSHV BAC16 Wild-type and Recombinant Virus**

257 Each population of BAC16-iSLK cells were reactivated using 1 ug/mL Doxycycline (Dox,
258 Sigma-Aldrich) and 1 mM NaB in antibiotic-free 10% FBS DMEM. At 72 or 96 hours post
259 infection, supernatants were collected and clarified at 4000 x *g* to remove cellular debris and
260 virus-containing supernatant stored at -80°C prior to use.

261 ***De novo* infection of Naïve HEK293T of HUVEC cells**

262 Sub-confluent (50-70%) 12-well plates of 293T or HUVEC cells were incubated with viral
263 inoculum diluted in antibiotic and serum free DMEM containing 8 $\mu$g/mL hexadimethrine
264 bromide (polybrene; Sigma-Aldrich). Plates were centrifuged at 800 x *g* for 2 hours at room
265 temperature (61), the inoculum was removed and replaced with either antibiotic-free 10% FBS
266 DMEM (293T) or full EGM-2 (HUVECs). Cells were then returned to the 37°C incubator.

267 **Immunofluorescence**

268 Cells were seeded onto 18mm round (#1.5, Electron Microscopy Sciences) coverslips, infected
269 or treated as noted for each experiment and fixed for 10 minutes at room temperature in 4% (v/v)

270 paraformaldehyde (Electron Microscopy Sciences) in PBS. Samples were permeabilized with
271 0.1% (v/v) Triton X-100 (Sigma-Aldrich) in PBS for 10 min at room temperature and blocked in
272 1% human AB serum (Sigma-Aldrich) for 1 hour at room temperature. Primary antibody was
273 diluted in 1% human AB serum (Sigma-Aldrich) in PBS at the concentrations in Table 2 and
274 incubated overnight. The following day secondary antibody was likewise diluted in 1% human
275 AB serum, alongside Hoechst (ThermoFisher Scientific) for nuclear staining, at the
276 concentrations in Table 2 and incubated for one hour. Samples were mounted with Prolong Gold
277 AntiFade mounting media (ThermoFisher Scientific). Images were captured using a Zeiss
278 AxioObserver Z1 microscope with the 40X objective unless otherwise stated.

279 **Image analysis**

280 Image analysis was performed using CellProfiler (cellprofiler.org), an open source software for
281 image analysis (62). Quantification of hedls/EDC4 and LANA-nuclear body (NB) puncta was
282 performed as previously described (63) with the following modifications. Rather than staining
283 cells with wheat germ agglutinin to identify cell periphery, individual cell cytoplasms were
284 defined based on a 150 pixel propagation away from the Hoescht-stained nucleus. The number of
285 Hedls/EDC4 puncta within a defined cell cytoplasm was reported. To quantify the number of
286 puncta in KSHV-infected cells, a gating strategy was applied to include only cells with LANA-
287 positive nuclei and defined cell cytoplasms for Hedls/EDC4 puncta quantification. LANA-NBs
288 were defined by thresholding and size was measured using the "MeasureObjectSizeShape"
289 function, respectively. Object area refers to the number of pixels within the identified region. At
290 least 50 cells were quantified for each condition.

291 **Immunoblotting**

292 Cells were lysed in 1x Laemmli buffer (4% SDS, 20% glycerol, 120 mM Tris-Cl (pH 6.8) and
293 $ddH_20$) and stored at -20°C until use. The DC Protein Assay (Bio-Rad) was used to quantify total
294 protein concentration as per the manufacturer's instructions. 10-15 µg of protein lysate was
295 resolved by SDS-PAGE on TGX Stain-Free acrylamide gels (BioRad). Membranes were blocked
296 in 5% BSA or 5% skim milk in Tris buffered saline-Tween20 (TBS-T). Primary and secondary
297 antibodies were diluted in 2.5% BSA or 2.5% skim milk, dilutions can be found in Table 1.
298 Membranes were visualized using ProtoGlow ECL (National Diagnostics) and the ChemiDoc
299 Touch Imaging system (BioRad).

300 **Intracellular viral genome qPCR**

301 Confluent 6-well plates of BAC16-iSLK.RTA cells were lysed using a DNeasy Blood and Tissue
302 Kit (Qiagen) according to manufacturer's protocol. Isolated DNA was stored at -20°C until
303 further use. DNA was diluted 1:30 prior to qPCR amplification using SsoFast EvaGreen
304 Supermix (Bio-Rad) and viral ORF26 or cellular β-actin (control) primers as listed in Table 3.
305 Fold change in viral genome copy number was determined using the ΔΔ-Quantitation cycle (Cq)
306 method.

307 **Dnase-protected viral genome qPCR**

308 Supernatants from reactivated iSLK cells were harvested and clarified at 4000 x *g* for 5 minutes.
309 Aliquots of 180 µL were stored separately at -80°C prior to use. Supernatants were thawed at
310 37°C and mixed with 20 µL of a 500U DNaseI (NEB), 10X buffer and nuclease free water
311 mixture and incubated at 37°C for 30 minutes. DNA was then extracted using a DNeasy Blood
312 and Tissue Kit with the following adjustments: per sample, 500 µg of salmon sperm DNA
313 (Invitrogen) and 1 ng of a luciferase (*luc2*) containing plasmid (pGL4.26, Clontech) was added

314 to buffer AL prior to lysis. DNA was not diluted prior to qPCR amplification using SsoFast
315 EvaGreen Supermix (Bio-Rad) and viral ORF26 and *luc2* (control) primers as listed in Table 3.
316 Since every viral particle contains one genome, and one genome contains a single copy of the
317 ORF26 gene, the number of viral DNA molecules could be calculated. Fold change in viral
318 DNase-protected genomes was determined using the ΔΔ-Quantitation cycle (Cq) method.

319 **Statistics**

320 Data shown are the mean ± standard deviation (SD). Statistical significance was determined
321 using a repeated measures 1-way ANOVA with a Dunnett's post-hoc test or simple linear
322 regression analysis. *P* values are indicated in figures, (*, $P < 0.05$; **, $P < 0.01$; ***, $P < 0.001$;
323 ns, nonsignificant). All statistics were performed using GraphPad Prism version 9.0.1.

324 **Data Availability**

325 All BAC16 virus sequences were deposited in the NCBI Sequence Read Archive (SRA) and are
326 accessible through the following SRA accession numbers: SAMN19671530 (WT KSHV
327 BAC16), SAMN19671876 (KSHV BAC16 ΔKapABC), SAMN19671877 (KSHV BAC16
328 ΔKapBC), SAMN19671902 (KSHV BAC16 ΔKapB), SAMN19672118 (KSHV BAC16
329 ΔKapC) and SAMN19672119 (KSHV BAC16 1X DRs).

330 **Results:**

331 **Construction of a panel of kaposin recombinant BAC16 KSHV viruses**

332 Work on the *kaposin* locus has been limited by the lack of recombinant viruses that target
333 this region. To address this limitation, we created a panel of recombinant viruses that delete
334 KapA, KapB and KapC individually or in combination. These recombinant viruses were created
335 using the KSHV bacterial artificial chromosome clone BAC16, which contains the pBelo45
336 plasmid inserted between the vIRF-1 and ORF57 genes of the JSC-1 KSHV isolate (58, 64). This
337 insertion encodes a red fluorescent protein (RFP) and a hygromycin resistance gene under the
338 control of a constitutive cellular promoter, to enable visual and chemical selection of BAC16-
339 containing cells, respectively. The wildtype (WT) kaposin mRNA encodes three open reading
340 frames (ORFs), KapA, KapB and KapC (Figure 1A). As a first step to create viruses that no
341 longer made one or more of these protein products, we removed the DR regions that encompass
342 the entire KapB ORF and most of the KapC ORF; in so doing, we created BAC16ΔKapBC. We
343 then mutated the KapA start codon in the context of BAC16ΔKapBC to create
344 BAC16ΔKapABC. However, creating single deletions of KapB and KapC by simple start codon
345 mutagenesis proved to be extremely difficult due to the GC-rich and repetitive nature of this
346 region. We decided to use an amino acid recoding strategy to construct BAC16 genomes that
347 failed to code for either KapB or KapC, but not both. While both ORFs are comprised largely of
348 23-nucleotide DRs that translate into 23-amino acid DRs, the ORFs are in different reading
349 frames. Using the BAC16 genome (accession #GQ994935), we designed two different gene
350 blocks with the nucleotide sequence of the DRs recoded. The first DNA construct was composed
351 of alternative codons that disrupted the protein coding capacity of the KapB ORF, due to several
352 nonsynonymous or nonsense mutations in the DRs but contained only synonymous nucleotide

353 changes in the KapC ORF that did not disrupt its amino acid sequence (ΔKapB; Figure 1B). The
354 second gene block coded for the inverse mutant; DRs were re-coded such that the KapC ORF
355 contained nonsynonymous or nonsense mutations, while the KapB ORF contained synonymous
356 mutations that did not disrupt its amino acid sequence (ΔKapC; Figure 1B). This strategy also
357 drastically decreased the GC-content of DR region from 78% to 59.6% or 63.3% for ΔKapB and
358 ΔKapC, respectively, facilitating the Lambda Red-based recombination events that followed and
359 enabling us to use colony PCR screening during mutagenesis.

360 We then tried to build a revertant in which the wild-type DRs were added back to
361 ΔKapBC to verify that off-target mutations did not occur during recombination. Our attempts to
362 re-insert full-length KapB/C ORF-containing DRs were unsuccessful, which we suspect is due to
363 recombination with the GC-rich, repetitive nucleotide constructs that led to partial or incomplete
364 recombination products, but also due to the difficulty in screening the successful recombination
365 of a GC-rich and repetitive region by colony PCR. However, we were able to successfully
366 reinsert a "mini" kaposin region comprised of 1 copy (23 amino acids) of each DR into the
367 ΔKapBC virus. The annotated wild-type (WT) BAC16 *kaposin* locus (accession #GQ994935)
368 contains 9 and 7 copies of DR1 and DR2 respectively; therefore, we called this "mini-revertant"
369 BAC16-1X DRs (Fig 1D). Previous work showed that ectopic expression of "mini" KapB,
370 containing 1X DRs, retained some functionality (46), justifying its utility herein.

371 A two-step lambda Red-based recombination method in *E.coli* was used to facilitate
372 BAC16 mutagenesis (Fig 1C) (65). In the first round, we introduced our desired mutation
373 adjacent to a KanSacB cassette for easy selection of successful recombinant BACmids. Colonies
374 that grew in the presence of kanamycin were verified by colony PCR to confirm recombination.
375 Using primer sets that bound the *kaposin* locus internally and externally, we were able to verify

376 both the orientation and size of each insert. In the second round of recombination, the KanSacB
377 cassette was removed, leaving only the desired mutation behind. Colonies that were screened
378 after this step were no longer sensitive to growth on 5% sucrose, as they had lost SacB, but were
379 rendered kanamycin sensitive. Colonies which grew accordingly were then screened using the
380 externally binding primer set, to confirm the correct size of each insert following KanSacB
381 removal and PCR products were sequenced by Sanger sequencing to confirm the desired
382 mutation had occurred within the *kaposin* locus.

383 We next isolated each recombinant BACmid from *E.coli* and performed whole genome
384 sequencing (WGS). Mapping of reads to the BAC16 reference genome (NCBI accession
385 #GQ994935) using Geneious Prime (60) revealed an average coverage per nucleotide of between
386 670 and 1430x. Subsequent analysis of variants revealed that no off-target mutations had
387 occurred during recombination (Figure 2A). Few variants were observed and these occurred
388 within repetitive regions of the KSHV genome that also displayed low coverage, as previously
389 shown (66–68). Outside of these, the only other variants detected were located in the region
390 between the genes for vIRF-1 and ORF57 (Figure 2A). This is to be expected, as this is where
391 the pBelo45 plasmid was inserted to facilitate the creation of BAC16, thereby altering the wild-
392 type nucleotide sequence in this genomic location (58). We focused our attention to the kaposin
393 DRs in WT BAC16. The repetitive nature of this sequence makes it difficult to resolve by WGS
394 (69) and we observed low coverage. There was no coverage in the DR region for both
395 ΔKapABC and ΔKapBC constructs, consistent with the complete removal of the DRs (Figure
396 2A). In contrast, we observed high read coverage of the recoded kaposin regions in ΔKapB and
397 ΔKapC viruses as recoding decreased the repetitive and GC-rich nature of the DRs (Figure 2B,
398 only WT and ΔKapB shown for simplicity). The consensus sequences produced for these regions

399 matched our recoded gene blocks, reaffirming successful recombination. Given the difficulty in
400 resolving DR regions through Illumina sequencing (69), we also checked the BAC16 genomes
401 using restriction fragment length polymorphism. BAC16 DNA isolated from *E.coli* was digested
402 using the restriction enzyme NheI, followed by pulse field gel electrophoresis (PFGE) to resolve
403 fragments. We observed fragment sizes consistent with predictions from *in silico* analysis using
404 NCBI accession #GQ994935 with the exception of the fragment comprised largely of terminal
405 repeats (TRs). We predicted that the TR-containing fragment should migrate at 33 kbp; however,
406 we did not observe a fragment of this size and instead observed an unexpected fragment
407 migrating at approximately 18 kbp. This suggested a deletion of approximately 15 kbp, or 19
408 copies of the 801bp sequence, within this region. This deletion has previously been observed in
409 BAC16 (70) because the highly repetitive nature of the TRs, as well as their high GC-content,
410 renders them sensitive to recombination events (71, 72). The altered size of the TR fragment was
411 found in WT BAC16 and in all five recombinant viruses, suggesting the event occurred prior to
412 our mutagenesis. PFGE analysis also revealed a second size discrepancy within the predicted
413 kaposin-containing fragment which WGS was unable to resolve due to the repetitive nature of
414 the region. Based on *in silico* analysis, we expected a 1200 bp fragment, yet the digestion of our
415 WT BAC16 genome produced a 1000 bp fragment. This suggests that over time the WT BAC16
416 construct lost 200bp, or approximately three 23-amino acid repeats, within the DR region,
417 making our recoded kaposin locus in ΔKapB and ΔKapC viruses longer than the kaposin locus in
418 WT BAC16. Because different KSHV isolates possess variable numbers of repeats (45), it is not
419 surprising to observe that this repetitive genomic area experienced DR contraction during
420 BAC16 DNA copying, like has been observed for the *kaposin* locus in KSHV. In future studies,

421 we hope to decipher whether there is any functional significance to the number of each kaposin
422 DR1 and DR2 for KSHV replication.

423 **Generation of stable BAC16-iSLK.RTA cell lines**

424 After sequencing, the BAC16 mutant genomes were used to generate stable iSLK cell
425 lines. A workhorse cell line for KSHV research, iSLK cells have been engineered to express the
426 viral lytic switch protein, RTA, in a Doxycycline (Dox)-inducible manner (59). These cells are
427 especially useful for KSHV research as they maintain tight control of latency and produce large
428 quantities of virus following the addition of Dox (59). However, iSLK cells were refractory to
429 transfection in our hands; thus, we first transfected BAC16 DNA into 293T cells to create stable
430 BAC16-293Ts for each BACmid (Figure 3A), as in (70). The efficiency of 293T transfection
431 was between 20-30%, as estimated by RFP expression. We gradually selected the transfected
432 cells with hygromycin until a confluent monolayer of RFP+ 293T cells was achieved (Figure
433 3B). Via quantitative PCR (qPCR) for viral DNA (ORF 26), we analyzed intracellular genome
434 copy number for each kaposin-deficient recombinant and found that intracellular genome copy
435 number was similar to WT in each case (Figure 3C).

436 BAC16-containing 293T cells were then co-cultured with naïve iSLKs and reactivated
437 using a histone deacetylase inhibitor (NaB) and a protein kinase C agonist (TPA) to produce
438 progeny virions (73–76). All kaposin-deficient viruses were able to infect naïve iSLKs judging
439 by RFP expression. The population of kaposin-deficient latent iSLK cells for each recombinant
440 was then expanded via gradual selection in the presence of hygromycin to eliminate uninfected
441 cells and puromycin to eliminate BAC16-293T cells, until a confluent layer of RFP-positive cells
442 was achieved (Figure 3D). Immediately after selection, we analyzed the features of our iSLK
443 latent cell lines. RFP-positive iSLKs cells were then stained by immunofluorescence to visualize

444 the viral latent protein LANA, which forms nuclear puncta called LANA nuclear bodies (NBs)
445 during KSHV infection (9–12) that were visible in all our kaposin-deficient latent iSLK cell lines
446 (Figure 3E), suggesting latency was successfully established. Using qPCR to quantify
447 intracellular genome copy number of our panel of latent iSLKs, we revealed that kaposin-
448 deficient iSLKs contained 10-40% of the genome copies observed in latent WT iSLKs (Figure
449 3F). These observations suggest the possibility that KSHV recombinant viruses that lack the
450 *kaposin* locus display defects in their ability to establish latency and/or undergo genome
451 amplification immediately following *de novo* infection, a step that serves to increase latent
452 episome copy number (6, 7).

453 Considering the possibility that *kaposin*-deficient KSHV recombinant viruses could be
454 less efficient at maintaining KSHV latency once already established, we decided to test how well
455 each latent cell population would maintain the viral genome compared to WT BAC16 latent
456 iSLKs in the absence of selective pressure. We passaged each latent cell line fifteen times in the
457 absence of hygromycin and determined intracellular genome copy number at each passage.
458 While WT BAC16 iSLKs displayed minimal episome loss over 15 passages (14, 77), we
459 observed that three of our kaposin-deficient recombinant viruses displayed accelerated genome
460 loss: ΔABC, ΔBC, and 1XDRs revertant whereas ΔKapB and ΔKapC genome copy number
461 remained steady over time (Figure 4A-B). Taken together with Figure 3, these data suggest that
462 the *kaposin* locus is important for the establishment of KSHV latency and may also contribute to
463 its maintenance.

464 **Cells latently infected with kaposin-deficient viruses produce progeny virions when**
465 **reactivated**

466 Having created latently infected iSLK cell lines for each of our recombinant viruses, we
467 first confirmed the absence of KapB and/or KapC protein products after 24 hours of reactivation
468 of our ΔABC, ΔBC, and ΔB/ΔC latent iSLK cell lines by immunoblotting with a DR1-specific
469 antibody (45) (Figure 5A). WT-infected cells exhibited a range of DR-specific banding as has
470 been previously observed, suggesting additional isoforms of KapB or KapC can be translated
471 (45, 46). Predominant bands at approximately 41kDa and 35kDa corresponded to the predicted
472 molecular weights of full-length KapC and KapB, respectively. As expected, due to the absence
473 of DR1 epitopes in these mutants, no KapB or KapC protein was detected in lysate from
474 reactivated ΔKapABC or ΔKapBC iSLKs. We observed a faint band was detected at ~46kDa in
475 lysate derived from ΔKapB-infected iSLKs which corresponds to the predicted molecular weight
476 of re-coded KapC (Figure 4A). This version of KapC is larger than that encoded by our WT
477 BAC16 because of the loss of DRs in our version of WT BAC16 (Figure 2). A prominent band
478 was consistently observed at ~42kDa in lysate from ΔKapC-infected iSLKs which corresponds
479 to the predicted molecular weight of re-coded KapB (Figure 5A), also larger than WT-derived
480 KapB for the same reason (Figure 2). No bands were observed in lysate from 1X DRs-infected
481 iSLK cells; we predict this is because there is only one DR1 epitope in this small protein. We
482 attempted to produce an IgY specific antibody (78) to recognize KapA; however, the antibody
483 failed to detect KapA in WT infection, making it not useful for our studies.

484 To determine if each of our kaposin-deficient iSLK cell lines was capable of reactivation,
485 completion of a full lytic replication cycle, and the production of progeny virions, we reactivated
486 the cell lines with Dox, to activate RTA expression, and NaB and measured intracellular genome
487 copy number by qPCR at 24, 48, 72, and 96 hours post reactivation. Genome copy number at
488 each time point was normalized to its matched starting genome copy number in latency since

489 each of the latent cell lines had a different episome copy number (Figure 3F) prior to
490 reactivation. For all recombinants, viral genome copy number significantly increased between 48
491 and 72 hours after reactivation (Figure 5B). WT and ΔKapB viruses exhibited ~15-fold increase
492 in intracellular genome copy number over latent copy number, ΔKapABC, ΔKapC and 1X DRs
493 viruses demonstrated a ~40-fold increase, and ΔKapBC virus genome copy number increased
494 ~200-fold by 96 hours post reactivation. We then determined how the reactivation process
495 altered viral genome copy number for each kaposin-deficient recombinant relative to WT and
496 observed that all kaposin-deficient viruses except for ΔKapB reached the same relative genome
497 copy number as WT by 96 hours post reactivation despite starting with less genomes than WT
498 (Figure 5C). These data show that all kaposin-deficient viruses are capable of genome replication
499 to increase viral DNA copy number after reactivation. Because the starting point of the
500 reactivation process was unequal in latency (Figure 3G), we were hesitant to draw quantitative
501 conclusions about the efficiency of genome replication after reactivation between our panel of
502 kaposin-deficient viruses.

503 We next determined if kaposin-deficient reactivated iSLK cells released progeny virus
504 particles into the media. To do so, we harvested the virus-containing supernatant at 96 hours post
505 reactivation and subjected it to DNase digestion to eliminate unencapsidated viral DNA, then
506 lysed the remaining encapsidated viruses, extracted the capsid-protected DNA and conducted
507 qPCR for viral DNA (Figure 5D). We found that kaposin-deficient viruses released similar
508 numbers of DNase-protected viral genomes to WT apart from the 1X DRs revertant which was
509 decreased 10-fold compared to WT (Figure 5D). Although this observation suggests that the
510 ability to package genomic material, assemble and release progeny virus does not require the
511 *kaposin* locus, we and others have observed that extracellular genome copy number does not

512 always correlate with infectious virus (21). To determine whether released virus from each
513 kaposin-deficient latent iSLK cell line were competent to infect naïve cells, we incubated a naïve
514 monolayer of 293T cells with supernatant from reactivated iSLK cells and 24 hours later, stained
515 cells for the latent protein LANA. We identified LANA-expressing cells in all 293T cell
516 monolayers infected by the panel of kaposin-deficient recombinant viruses, (Figure 5E) showing
517 that each kaposin-deficient virus can produce infectious progeny virions. This is consistent with
518 our earlier observations using the 293T-iSLK co-culture system, as this method of latent cell line
519 creation relies on successful lytic replication and virion production.

520 **Latent iSLK cells that lack Kaposin B display altered latency phenotypes**

521 Previous work from our lab used ectopic overexpression of KapB to characterize its
522 function independent of viral infection. Consequently, we were most interested in analyzing the
523 behaviour of the ΔKapB recombinant virus. We reactivated WT and ΔKapB-BAC16 iSLKs to
524 produce progeny virus, equalized extracellular genomic copy number, and infected naïve cells for
525 24 hours; however, we saw very few LANA-positive cells post infection (Figure 6A). Given the
526 inconsistencies between stable BAC16 cell lines reported by others (79, 80), we decided to re-
527 derive another ΔKapB-latent iSLK cell line. Using the same population of ΔKapB-BAC16-
528 transfected 293Ts cells and an identical protocol for co-culture, selection and expansion, we
529 produced a new ΔKapB iSLK cell line that we will refer to as ΔKapB-2 iSLKs, while our
530 original ΔKapB iSLK cell line will be referred to as ΔKapB-1. Following ΔKapB-2 iSLK
531 reactivation, we noticed a greater cytopathic effect in reactivated ΔKapB-2 iSLKs than
532 previously observed in reactivated ΔKapB-1 iSLKs. We then equalized extracellular particle
533 number as above, infected naïve cells with ΔKapB-2 BAC16 and observed a 2-fold reduction in
534 LANA-positive cells compared to WT virus (Figure 6B), a great improvement compared to

535 ΔKapB-1. The large difference between infectious progeny production from ΔKapB-1 versus
536 ΔKapB-2 latent iSLKs prompted us to derive two additional ΔKapB iSLK cell lines as described
537 above, termed ΔKapB-3 and ΔKapB-4. We compared several features between these four
538 ΔKapB iSLK cell lines. We noted that although all four latent cell lines were RFP-positive,
539 ΔKapB-1 latent iSLK cells did not fluoresce as brightly as WT or the other ΔKapB latent cell
540 lines (Figure 6C). We stained these latent cells for LANA nuclear bodies (NBs) and observed
541 several differences between LANA NBs present in latent WT iSLKs compared to the four
542 ΔKapB latent iSLK cell lines (Figure 6D). Although WT latent cells had fewer LANA NBs per
543 cell than all four ΔKapB latent cell lines (Figure 6E), WT LANA NBs averaged a much larger
544 area than in ΔKapB latent cell lines (Figure 6F). Of the four ΔKapB latent cell lines, ΔKapB-4
545 displayed LANA NB character that most closely resembled WT; namely, fewer LANA NBs that
546 were brighter and larger (Figure 6D-F). However, all four ΔKapB latent cell lines showed
547 episome copy number ~10-25% that of WT latent iSLKs (Figure 6G). Of these, ΔKapB-2 and
548 ΔKapB-4 had the higher genome copy number, consistent with ΔKapB-2 iSLK improved
549 reactivation (ΔKapB-2, Figure 6B) and ΔKapB-4 iSLK LANA NB character (ΔKapB-4, Figure
550 6D-F). In addition, all four ΔKapB latent cell lines displayed reduced steady-state levels of
551 LANA protein compared to WT (Figure 6H). Taken together, these distinct differences clustered
552 the four ΔKapB iSLK latent cell lines as defective compared to WT in terms of key latency
553 phenotypes such as LANA NB area, steady-state levels of LANA protein, and KSHV genome
554 copy number.

555 **KapB is required for processing body disassembly after *de novo* infection of HUVECs**

556 We have previously shown that ectopic expression of KapB in human umbilical vein
557 endothelial cells (HUVECs) is sufficient to recapitulate key phenotypes associated with KSHV

558 latency, including the disassembly of processing bodies (PBs), cytoplasmic RNA and protein
559 granules whose loss correlates with enhanced inflammatory cytokine RNAs (51, 53–57). To
560 determine if KapB was necessary for KSHV-induced PB loss, we reactivated ΔKapB-2 latent
561 iSLK cells and used this virus to infect HUVECs. After 96 hours post infection, we fixed the
562 infected cells and stained the monolayer for both LANA and for a PB-resident protein called
563 Hedls/EDC4 (81, 82). We observed that ~80-90% of the cell monolayer was infected with either
564 ΔKapB BAC16 or WT BAC16 virus. In LANA-positive cells that were infected with WT virus,
565 we observed a two-fold decrease in PBs per infected cell compared to the mock-infected control
566 (Figure 7A-B), as shown previously (51). In LANA-positive cells infected with ΔKapB-2 virus,
567 PB numbers were not significantly altered relative to the mock-infected control (Figure 7A-B).
568 We also confirmed that WT-infected HUVECs expressed KapB, but that KapB was absent in
569 ΔKapB-infected HUVECs (Figure 7C). These data reveal for the first time that the KapB protein
570 is required for KSHV-induced PB disassembly following *de novo* infection.

571 We previously showed that ectopic expression of KapB is sufficient to induce primary
572 ECs to elongate and spindle, thereby recapitulating the morphology of infected cells within KS
573 lesions (51, 83). However, others have observed that ectopic expression of v-FLIP likewise
574 elicits EC spindling (84) and that the deletion of v-FLIP from the viral genome eliminates EC
575 spindling, although this effect is overcome at high multiplicity of infection (85). To test if KapB
576 is necessary for EC spindling, we used WT of ΔKapB BAC16, derived as above, to infect
577 HUVECs, fixed cells at 96hpi and visualized spindling at low magnification by brightfield
578 microscopy or at high magnification by staining fixed cells with phalloidin to label actin
579 filaments. Robust cell spindling was observed in LANA-positive, WT-infected cells (Figure 7D).
580 We also observed spindled cells in LANA-positive, ΔKapB-infected HUVECs (Figure 7D). We

581 conclude that although ectopic expression of KapB is sufficient to elicit EC spindling (51), it is

582 not necessary for EC spindling during KSHV latency.

583 **Discussion:**

584 The kaposin locus comprises a significant portion of the coding capacity of the KSHV
585 latency locus, yet its role in KSHV latent and lytic replication is not fully appreciated. Prior to
586 this report, the KSHV field lacked recombinant viruses to enable functional analysis of
587 individual kaposin proteins in the context of KSHV infection. Here we described the
588 construction and validation of a suite of kaposin-deficient recombinant viruses using the BAC16
589 bacterial artificial chromosome and a panel of corresponding stable iSLK cell lines. We deleted
590 or recoded kaposin ORFs individually or in combination, generating several mutants: ΔKapABC,
591 ΔKapBC, ΔKapB, ΔKapC and a partial revertant, 1xDRs. We showed that all kaposin-deficient
592 viruses are capable of establishing latency in iSLKs, replicating the viral genome upon
593 reactivation, and producing progeny virions that can be used for *de novo* infection of naïve cells.
594 Despite this, all kaposin-deficient latent iSLK cells lines displayed reduced viral genome copy
595 number during latency compared to WT. In addition, we characterized four derivations of
596 ΔKapB-iSLKs and showed that these cells not only have markedly reduced genome copy
597 number, but also reduced LANA NB area and LANA protein level. Together, these data suggest
598 that the kaposin locus plays a role in latency establishment. Finally, we used ΔKapB BAC16 to
599 show that KapB is not only sufficient but also necessary for KSHV-mediated PB disassembly
600 following *de novo* infection of primary ECs, verifying the contribution of an individual kaposin
601 protein to KSHV biology. This toolkit will allow us to interrogate the role of the kaposin locus in
602 KSHV replication with unprecedented precision, making it a significant advance for the field.

603 Previous knowledge about the role of the kaposin locus was derived from studies using
604 the ectopic expression of individual kaposin ORFs (47, 51, 52, 86–88). To date, no
605 comprehensive kaposin-deficient BAC16 studies have been published. Toth *et al*., created a

606 kaposin knockout BAC16 virus by deleting a 1319-nucleotide region that included the coding
607 region of KapA and the majority of the coding regions of KapB and KapC (89). This
608 recombinant virus was used to test for the recruitment of proteins from polycomb repressive
609 complexes 1 and 2 to two lytic viral promoters after primary infection of SLK cells (89). For this
610 phenotype, the kaposin knockout virus displayed no difference from WT, but aside from this, no
611 additional analyses related to this mutant were reported. Gallo *et al.* created a K12 mutant in
612 which a kanamycin cassette disrupts the K12 ORF, but reported limited phenotypic analysis
613 related to this virus (90). Finally, Campbell *et al*. investigated the role of the RTA-responsive
614 element (RRE) promoter in the kaposin locus, and in so doing created a K12 RRE-mutant;
615 however, this study focused solely on RTA-recruitment and genomic architecture (91). In the
616 current study, our recombinant viruses were created by removing all DR1 and DR2 sequences
617 (ΔKapBC) with or without mutagenesis of the KapA ORF start codon (ΔKapABC), or by
618 replacing the DR region with alternatively coded nucleotide sequences (ΔKapB and ΔKapC).
619 Our recoding strategy had several advantages. First, the translation potential of the *kaposin* locus
620 was reduced by insertion of multiple termination codons, eliminating expression of some protein
621 products while maintaining other ORFs by alternative codon usage. Second, recoding destroyed
622 the repetitive nature of the locus and decreased the GC-content, making the region much more
623 amenable to error-free homologous recombination. Third, in all of the recombinant kaposin-
624 mutant BACs, regulatory sequences for transcription and miRNA processing were left intact. We
625 also created corresponding latent iSLK cell lines for the kaposin-deficient BAC16 constructs. All
626 four of these kaposin-deficient latent iSLK cell lines showed drastic reductions in viral genome
627 copy number compared to WT. The cell lines were created by co-culturing BAC16-transfected
628 HEK 293Ts with naïve iSLKs, a widely used method reported to be more efficient than direct

629 transfection of recombinant BAC16 DNA, that leverages cell-to-cell spread of virions from
630 reactivated 293T cells to iSLKs (5, 59, 70, 92). Despite using this strategy, we failed to produce
631 latent cell lines that contained high genome copy numbers for any of the kaposin-deficient
632 BAC16 DNA. We repeated the co-culture procedure for the most impaired of these four times,
633 and each attempt yielded similar results; all four ΔKapB iSLK cell lines displayed reduced viral
634 episome number and altered LANA NBs compared to WT BAC16 cells. Although these data are
635 consistent with the idea that kaposin-deficient viruses are impaired in one or more key steps
636 required for the establishment of latency, further study is required to characterize the nature of
637 this defect.

638 LANA expression and function is central to the establishment of KSHV latency. LANA
639 forms homo-oligomers and binds the terminal repeat (TR) regions of the KSHV genome while
640 simultaneously binding histones H2A and H2B of host chromatin, thereby tethering the viral
641 DNA to host chromosomes (8, 10, 11, 93). This binding leads to the formation of structures
642 called LANA NBs that colocalize with viral genomes (10, 94, 95). The number of LANA-
643 positive puncta in an infected cell correlates with the number of viral episomes (13). KSHV *de*
644 *novo* infection of a cell monolayer is heterogenous and results in variable levels of intracellular
645 viral genomes between individual latent cells, and this heterogeneity is also represented by
646 diverse LANA NB number per cell (13). Therefore, robust LANA NB staining is a marker for
647 successful latency establishment. We and others have observed heterogenous LANA NB size
648 within and between latent infected cells; however, the significance of this size variability is less
649 clear. Because LANA can bind to nucleosomes in cellular chromosomes as well as those bound
650 to viral episomes (15), LANA NBs are classified as supramolecular structures that cluster
651 multiple viral episomes together (12, 95). Genome clustering was proposed to be an effective

652 evolutionary strategy that allows KSHV to rapidly increase viral genome copy number per cell at
653 the expense of total number of cells infected (15). It is not yet clear if a minimum number of
654 viral episomes are required to create a supramolecular LANA NB after *de novo* infection;
655 however, WT KSHV does preferentially form clustered LANA NBs (15). We have observed that
656 latent ΔKapB iSLK cells possess LANA NBs that are less diverse in terms of size, and overall
657 much smaller than LANA NBs in WT iSLK cells. Therefore, we report an additional correlative
658 phenotype between low genome copy number and smaller LANA NBs observed in multiple
659 derivations of ΔKapB latent iSLK cell lines and speculate that ΔKapB iSLK cells do not contain
660 enough viral episomes to form large LANA NBs with clustered genomes.

661 The kaposin locus overlaps with one of two possible viral origins of lytic genome
662 replication, called OriLytR. Though very few studies have interrogated the contribution of
663 OriLytR/kaposin to viral genome replication, detailed analyses on the function of OriLytL have
664 revealed that it facilitates genome copying after viral reactivation and upon *de novo* infection
665 (96–99). More recent work has shown an essential role for OriLytL transcription in viral genome
666 replication after *de novo* infection (99). We speculate that loss of the GC-rich kaposin repeat
667 region in our mutants impairs the contribution of OriLytR to viral genome copying that occurs
668 after *de novo* infection, as was observed for a recombinant virus lacking OriLytL (99). A
669 reduction in viral genome copy number after *de novo* infection would be predicted to impair
670 latency establishment and diminish the clustering of viral episomes into larger LANA NBs,
671 which may explain the different LANA NB phenotype we observed in all four ΔKapB iSLK
672 latent cell lines. At odds with our model is that the loss of the kaposin region does not appear to
673 negatively impact viral genome replication after reactivation. We speculate that this step is not as
674 sensitive to the loss of one of two functional origins of lytic replication, as also observed for loss

675 of OriLytL. Further experimentation will be needed to reveal the precise mechanism by which
676 kaposin DR repeats may modulate viral abortive lytic replication and how this may impact
677 LANA NB formation, function and latency establishment.

678 KSHV latency predominates in most cells in culture and in KS tumours, suggesting viral
679 proteins expressed at this time are important in promoting tumourigenesis. We have previously
680 shown that ectopic expression of KapB in primary ECs recapitulates two features of the KS
681 lesion: cell spindling and elevated inflammatory cytokine expression via PB disassembly. Using
682 the ΔKapB BAC16 recombinant virus, we analyzed if KapB was not only sufficient but
683 necessary for these KSHV-associated tumor phenotypes. We show that after *de novo* infection of
684 HUVECs, ΔKapB BAC16 cells can induce cell spindling to a similar extent as WT BAC16
685 virus. These data are consistent with reports that the viral latent gene vFLIP is also capable of
686 causing endothelial cell spindling; therefore, the loss of KapB does not eliminate the spindling
687 phenotype (84). We propose that KapB and v-FLIP may act synergistically to promote EC
688 spindling during KSHV latency, and that in absence of one, the other is able to compensate. We
689 also used the ΔKapB BAC16 recombinant virus to determine if KapB was necessary for KSHV-
690 induced PB disassembly. PBs are cytoplasmic sites for the constitutive turnover or translational
691 suppression of ARE-containing inflammatory cytokine mRNAs (51, 53–57). We previously
692 showed that latent KSHV infection of primary ECs caused PB disassembly (51). Here, we also
693 observed that 96 hours after d*e novo* infection of HUVECs with WT BAC16, PBs were
694 disassembled. However, d*e novo* infection of HUVECs with ΔKapB BAC16 did not cause PB
695 disassembly. This reveals that KapB is both necessary and sufficient for PB disassembly during
696 KSHV latency and represents the first time that a phenotypic function can be specifically
697 attributed to a single kaposin protein in the context of KSHV infection.

698 Our group and others showed that PBs also decrease during lytic replication and that
699 more than one viral protein is sufficient for this effect (53, 100). Here, we observed PB
700 disassembly 96 hours after *de novo* infection of HUVECs, and we have previously shown PB
701 disassembly in latent HUVECs (51). In contrast, Sharma *et al.* reported that PBs were not lost in
702 a KSHV-infected latent primary effusion lymphoma cell line. This discrepancy could be
703 attributed to the use of B-lymphocytes in their studies or their visualization of PBs by staining
704 largely for the PB-resident protein GW182, an antigen that has been shown to adopt a punctate
705 pattern distinct from other PB marker proteins (100, 101). Taken together, the observation that
706 KSHV encodes multiple proteins in both phases of its replication to elicit PB disassembly
707 suggests the functional relevance of this phenotype for viral infection. Because PBs
708 constitutively repress many pro-inflammatory, angiogenic, or pro-tumourigenic cellular
709 transcripts, we propose that the absence of microscopically visible PBs may contribute to the
710 inflammatory and angiogenic KS microenvironment and that KapB is necessary for this effect in
711 KS lesions.

712 In summary, this work describes the construction and preliminary analysis of four
713 different kaposin-deficient BAC16 viruses and corresponding iSLK latent cell lines. We used
714 these mutants to specifically attribute the phenotype of PB disassembly following *de novo*
715 infection of primary to the viral protein KapB. This work also provides preliminary data to
716 suggest that the *kaposin* locus aids in the establishment of KSHV latency after primary infection,
717 a role that may suggest that the region derives function from its GC-rich direct repeats in
718 addition to its protein products. We hope these mutants will enable future studies to better
719 evaluate the roles of individual kaposin protein products during infection. Moreover, we believe

720 our strategy to recode protein products in multiple reading frames can serve as a mutagenesis

721 roadmap for understanding other complex, polycistronic viral loci.

722 **Acknowledgements**

723 We sincerely thank the members of the Corcoran lab for helpful discussions about this work
724 including Ms. Julie Ryu for designing recoded ΔKapB sequence. We would like to thank Dr.
725 Craig McCormick (Dalhousie University) for valuable feedback on this manuscript and the
726 McCormick lab for plasmids, expertise and advice. We would like to thank Dr. Anne Vaahtokari
727 of the Charbonneau Microscopy Facility, UCalgary for microscopy support. We would like to
728 thank Dr. John Archibald (Dalhousie University) and the Archibald lab for help performing
729 pulse-field gel electrophoresis and Dr. Jae Jung (Cleveland Clinic) for sharing the BAC16-RFP
730 bacterial artificial chromosome. MK was supported by a CSM graduate training award and a
731 CIHR CGS-M scholarship. GM was supported by a CRTP graduate training award. Operating
732 funds to support this work derive from a CIHR Project Grant PJT-153210 to JAC.

733

734 **Author Contributions**

735 Mariel Kleer: Conceptualization, Experimentation, Analysis, Paper Writing

736 Grant MacNeil: Conceptualization, Experimentation, Analysis

737 Eric S. Pringle: Conceptualization, Supervision

738 Jennifer A. Corcoran: Conceptualization, Experimentation, Supervision, Funding Acquisition,
739 Project Administration, Paper Writing

740

741 **Conflict of Interest**

742 The authors have no competing interests to declare.

743 **References**


744 1. Chang Y, Cesarman E, Pessin MS, Lee F, Culpepper J, Knowles DM, Moore PS. 1994.
745 Identification of herpesvirus-like DNA sequences in AIDS-associated Kaposi's sarcoma.
746 Science (80- ) https://doi.org/10.1126/science.7997879.

747 2. Cesarman E, Chang Y, Moore PS, Said JW, Knowles DM. 1995. Kaposi's sarcoma—
748 associated herpesvirus-like DNA sequences in AIDS-related body-cavity—based
749 lymphomas. N Engl J Med https://doi.org/10.1056/NEJM199505043321802.

750 3. Soulier J, Grollet L, Oksenhendler E, Cacoub P, Cazals-Hatem D, Babinet P, D'Agay MF,
751 Clauvel JP, Raphael M, Degos L, Sigaux F. 1995. Kaposi's sarcoma-associated
752 herpesvirus-like DNA sequences in multicentric Castleman's disease. Blood
753 https://doi.org/10.1182/blood.v86.4.1276.bloodjournal8641276.

754 4. Lagunoff M, Bechtel J, Venetsanakos E, Roy AM, Abbey N, Herndier B, Ganem D,
755 McMahon M, Ganem D. 2002. De Novo Infection and Serial Transmission of Kaposi ' s
756 Sarcoma-Associated Herpesvirus in Cultured Endothelial Cells. J Virol
757 https://doi.org/10.1128/JVI.76.5.2440.

758 5. Renne R, Blackbourn D, Whitby D, Levy J, Ganem D. 1998. Limited transmission of
759 Kaposi's sarcoma-associated herpesvirus in cultured cells. J Virol.

760 6. Purushothaman P, Thakker S, Verma SC. 2015. Transcriptome Analysis of Kaposi's
761 Sarcoma-Associated Herpesvirus during De Novo Primary Infection of Human B and
762 Endothelial Cells . J Virol https://doi.org/10.1128/jvi.02507-14.

763 7. Krishnan HH, Naranatt PP, Smith MS, Zeng L, Bloomer C, Chandran B. 2004.

764 Concurrent Expression of Latent and a Limited Number of Lytic Genes with Immune
765 Modulation and Antiapoptotic Function by Kaposi's Sarcoma-Associated Herpesvirus
766 Early during Infection of Primary Endothelial and Fibroblast Cells and Subsequent
767 Decline of L. J Virol https://doi.org/10.1128/jvi.78.7.3601-3620.2004.

768 8. Cotter MA, Robertson ES. 1999. The latency-associated nuclear antigen tethers the
769 Kaposi's sarcoma- associated herpesvirus genome to host chromosomes in body cavity-
770 based lymphoma cells. Virology https://doi.org/10.1006/viro.1999.9999.

771 9. Szekely L, Kiss C, Mattsson K, Kashuba E, Pokrovskaja K, Juhasz A, Holmvall P, Klein
772 G. 1999. Human herpesvirus-8-encoded LNA-1 accumulates in heterochromatin-
773 associated nuclear bodies. J Gen Virol https://doi.org/10.1099/0022-1317-80-11-2889.

774 10. Ballestas ME, Chatis PA, Kaye KM. 1999. Efficient persistence of extrachromosomal
775 KSHV DNA mediated by latency- associated nuclear antigen. Science (80- )
776 https://doi.org/10.1126/science.284.5414.641.

777 11. Schwam DR, Luciano RL, Mahajan SS, Wong L, Wilson AC. 2000. Carboxy Terminus of
778 Human Herpesvirus 8 Latency-Associated Nuclear Antigen Mediates Dimerization,
779 Transcriptional Repression, and Targeting to Nuclear Bodies. J Virol
780 https://doi.org/10.1128/jvi.74.18.8532-8540.2000.

781 12. De Leo A, Deng Z, Vladimirova O, Chen HS, Dheekollu J, Calderon A, Myers KA,
782 Hayden J, Keeney F, Kaufer BB, Yuan Y, Robertson E, Lieberman PM. 2019. LANA
783 oligomeric architecture is essential for KSHV nuclear body formation and viral genome
784 maintenance during latency. PLoS Pathog https://doi.org/10.1371/journal.ppat.1007489.

785 13. Adang LA, Parsons CH, Kedes DH. 2006. Asynchronous Progression through the Lytic

786 Cascade and Variations in Intracellular Viral Loads Revealed by High-Throughput Single-
787 Cell Analysis of Kaposi's Sarcoma-Associated Herpesvirus Infection. J Virol
788 https://doi.org/10.1128/jvi.01156-06.

789 14. Grundhoff A, Ganem D. 2004. Inefficient establishment of KSHV latency suggests an
790 additional role for continued lytic replication in Kaposi sarcoma pathogenesis. J Clin
791 Invest https://doi.org/10.1172/JCI200417803.

792 15. Chiu YF, Sugden AU, Fox K, Hayes M, Sugden B. 2017. Kaposi's sarcoma-associated
793 herpesvirus stably clusters its genomes across generations to maintain itself
794 extrachromosomally. J Cell Biol https://doi.org/10.1083/jcb.201702013.

795 16. Lukac DM, Renne R, Kirshner JR, Ganem D. 1998. Reactivation of Kaposi's sarcoma-
796 associated herpesvirus infection from latency by expression of the ORF 50 transactivator,
797 a homolog of the EBV R protein. Virology https://doi.org/10.1006/viro.1998.9486.

798 17. Lukac DM, Kirshner JR, Ganem D. 1999. Transcriptional Activation by the Product of
799 Open Reading Frame 50 of Kaposi's Sarcoma-Associated Herpesvirus Is Required for
800 Lytic Viral Reactivation in B Cells. J Virol https://doi.org/10.1128/jvi.73.11.9348-
801 9361.1999.

802 18. Xu Y, AuCoin DP, Huete AR, Cei SA, Hanson LJ, Pari GS. 2005. A Kaposi's Sarcoma-
803 Associated Herpesvirus/Human Herpesvirus 8 ORF50 Deletion Mutant Is Defective for
804 Reactivation of Latent Virus and DNA Replication. J Virol
805 https://doi.org/10.1128/jvi.79.6.3479-3487.2005.

806 19. Sun R, Lin S-F, Staskus K, Gradoville L, Grogan E, Haase A, Miller G. 1999. Kinetics of
807 Kaposi's Sarcoma-Associated Herpesvirus Gene Expression. J Virol

808 https://doi.org/10.1128/jvi.73.3.2232-2242.1999.

809 20. Sun R, Lin SF, Gradoville L, Yuan Y, Zhu F, Miller G. 1998. A viral gene that activates
810 lytic cycle expression of Kaposi's sarcoma-associated herpesvirus. Proc Natl Acad Sci U
811 S A https://doi.org/10.1073/pnas.95.18.10866.

812 21. Nakajima K, Guevara-Plunkett S, Chuang F, Wang K-H, Lyu Y, Kumar A, Luxardi G,
813 Izumiya C, Soulika A, Campbell M, Izumiya Y. 2020. Rainbow Kaposi's Sarcoma-
814 Associated Herpesvirus Revealed Heterogenic Replication with Dynamic Gene
815 Expression. J Virol https://doi.org/10.1128/jvi.01565-19.

816 22. Chen CP, Lyu Y, Chuang F, Nakano K, Izumiya C, Jin D, Campbell M, Izumiya Y. 2017.
817 Kaposi's Sarcoma-Associated Herpesvirus Hijacks RNA Polymerase II To Create a Viral
818 Transcriptional Factory. J Virol https://doi.org/10.1128/jvi.02491-16.

819 23. Okoid LM, Kimballid AK, Kasparid RE, Knoxid AN, Coleman CB, Rochford R, Chang
820 T, Alderete B, van Dyk LF, Clambey ET. 2019. Multidimensional analysis of
821 gammaherpesvirus RNA expression reveals unexpected heterogeneity of gene expression.
822 PLoS Pathog https://doi.org/10.1371/journal.ppat.1007849.

823 24. Zhong W, Wang H, Herndier B, Ganem D. 1996. Restricted expression of Kaposi
824 sarcoma-associated herpesvirus (human herpesvirus 8) genes in Kaposi sarcoma. Proc
825 Natl Acad Sci U S A https://doi.org/10.1073/pnas.93.13.6641.

826 25. Katano H, Sato Y, Kurata T, Mori S, Sata T. 2000. Expression and localization of human
827 herpesvirus 8-encoded proteins in primary effusion lymphoma, Kaposi's sarcoma, and
828 multicentric Castleman's disease. Virology https://doi.org/10.1006/viro.2000.0196.

829 26. Katano H, Sato Y, Itoh H, Sata T. 2001. Expression of human herpesvirus 8 (HHV-8)-
830 encoded immediate early protein, open reading frame 50, in HHV-8-associated diseases. J
831 Hum Virol.

832 27. Staskus KA, Gebhard K, Haase AT, Zhong W, Wang H, Renne R, Ganem D, Herndier B,
833 Beneke J, Pudney J, Anderson DJ. 1997. Kaposi's sarcoma-associated herpesvirus gene
834 expression in endothelial (spindle) tumor cells. J Virol.

835 28. Bais C, Santomasso B, Coso O, Arvanitakis L, Raaka EG, Gutkind JS, Asch AS,
836 Cesarman E, Gerhengorn MC, Mesri EA. 1998. G-protein-coupled receptor of Kaposi's
837 sarcoma-associated herpesvirus is a viral oncogene and angiogenesis activator. Nature
838 https://doi.org/10.1038/34193.

839 29. Montaner S, Sodhi A, Molinolo A, Bugge TH, Sawai ET, He Y, Li Y, Ray PE, Gutkind
840 JS. 2003. Endothelial infection with KSHV genes in vivo reveals that vGPCR initiates
841 Kaposi's sarcomagenesis and can promote the tumorigenic potential of viral latent genes.
842 Cancer Cell https://doi.org/10.1016/S1535-6108(02)00237-4.

843 30. Mazzi R, Parisi SG, Sarmati L, Uccella I, Nicastri E, Carolo G, Gatti F, Concia E,
844 Andreoni M. 2001. Efficacy of cidofovir on human herpesvirus 8 viraemia and Kaposi's
845 sarcoma progression in two patients with AIDS [1]. AIDS.

846 31. Mesri EA, Feitelson MA, Munger K. 2014. Human viral oncogenesis: A cancer hallmarks
847 analysis. Cell Host Microbe.

848 32. Martin DF, Kuppermann BD, Wolitz RA, Palestine AG, Li H, Robinson CA. 1999. Oral
849 Ganciclovir for Patients with Cytomegalovirus Retinitis Treated with a Ganciclovir
850 Implant. N Engl J Med https://doi.org/10.1056/nejm199904083401402.

851 33. Bravo Cruz AG, Damania B. 2019. In Vivo Models of Oncoproteins Encoded by
852 Kaposi's Sarcoma-Associated Herpesvirus . J Virol https://doi.org/10.1128/jvi.01053-18.

853 34. Friborg J, Kong WP, Hottlger MO, Nabel GJ. 1999. p53 Inhibition by the LANA protein
854 of KSHV protects against cell death. Nature https://doi.org/10.1038/47266.

855 35. Fujimuro M, Wu FY, Aprhys C, Kajumbula H, Young DB, Hayward GS, Hayward SD.
856 2003. A novel viral mechanism for dysregulation of β-catenin in Kaposi's sarcoma-
857 associated herpesvirus latency. Nat Med https://doi.org/10.1038/nm829.

858 36. Radkov SA, Kellam P, Boshoff C. 2000. The latent nuclear antigen of Kaposi sarcoma-
859 associated herpesvirus targets the retinoblastoma-E2F pathway and with the oncogene
860 Hras transforms primary rat cells. Nat Med https://doi.org/10.1038/80459.

861 37. Sin SH, Dittmer DP. 2013. Viral latency locus augments B-cell response in vivo to induce
862 chronic marginal zone enlargement, plasma cell hyperplasia, and lymphoma. Blood
863 https://doi.org/10.1182/blood-2012-03-415620.

864 38. Qin J, Li W, Gao SJ, Lu C. 2017. KSHV microRNAs: Tricks of the Devil. Trends
865 Microbiol.

866 39. Arias C, Weisburd B, Stern-Ginossar N, Mercier A, Madrid AS, Bellare P, Holdorf M,
867 Weissman JS, Ganem D. 2014. KSHV 2.0: A Comprehensive Annotation of the Kaposi's
868 Sarcoma-Associated Herpesvirus Genome Using Next-Generation Sequencing Reveals
869 Novel Genomic and Functional Features. PLoS Pathog
870 https://doi.org/10.1371/journal.ppat.1003847.

871 40. Sarid R, Flore O, Bohenzky RA, Chang Y, Moore PS. 1998. Transcription Mapping of the

872 Kaposi's Sarcoma-Associated Herpesvirus (Human Herpesvirus 8) Genome in a Body
873 Cavity-Based Lymphoma Cell Line (BC-1). J Virol https://doi.org/10.1128/jvi.72.2.1005-
874 1012.1998.

875 41. Dittmer D, Lagunoff M, Renne R, Staskus K, Haase A, Ganem D. 1998. A Cluster of
876 Latently Expressed Genes in Kaposi's Sarcoma-Associated Herpesvirus. J Virol
877 https://doi.org/10.1128/jvi.72.10.8309-8315.1998.

878 42. Schulz TF, Cesarman E. 2015. Kaposi Sarcoma-associated Herpesvirus: Mechanisms of
879 oncogenesis. Curr Opin Virol.

880 43. Dittmer DP, Damania B. 2016. Kaposi sarcoma-associated herpesvirus: Immunobiology,
881 oncogenesis, and therapy. J Clin Invest.

882 44. Rose TM, Bruce AG, Barcy S, Fitzgibbon M, Matsumoto LR, Ikoma M, Casper C, Orem
883 J, Phipps W. 2018. Quantitative RNAseq analysis of Ugandan KS tumors reveals KSHV
884 gene expression dominated by transcription from the LTd downstream latency promoter.
885 PLoS Pathog https://doi.org/10.1371/journal.ppat.1007441.

886 45. Sadler R, Wu L, Forghani B, Renne R, Zhong W, Herndier B, Ganem D. 1999. A complex
887 translational program generates multiple novel proteins from the latently expressed
888 kaposin (K12) locus of Kaposi's sarcoma-associated herpesvirus. J Virol.

889 46. McCormick C, Ganem D. 2006. Phosphorylation and Function of the Kaposin B Direct
890 Repeats of Kaposi's Sarcoma-Associated Herpesvirus. J Virol
891 https://doi.org/10.1128/jvi.02331-05.

892 47. Kliche S, Nagel W, Kremmer E, Atzler C, Ege A, Knorr T, Koszinowski U, Kolanus W,

893 Haas J. 2001. Signaling by human herpesvirus 8 kaposin a through direct membrane
894 recruitment of cytohesin-1. Mol Cell https://doi.org/10.1016/S1097-2765(01)00227-1.

895 48. Muralidhar S, Pumfery AM, Hassani M, Sadaie MR, Kishishita M, Brady JN, Doniger J,
896 Medveczky P, Rosenthal LJ. 1998. Identification of kaposin (open reading frame K12) as
897 a human herpesvirus 8 (Kaposi's sarcoma-associated herpesvirus) transforming gene. J
898 Virol.

899 49. Tomkowicz B, Singh SP, Cartas M, Srinivasan A. 2002. Human herpesvirus-8 encoded
900 kaposin: Subcellular localization using immunofluorescence and biochemical approaches.
901 DNA Cell Biol https://doi.org/10.1089/10445490252925413.

902 50. Forte E, Raja AN, Shamulailatpam P, Manzano M, Schipma MJ, Casey JL, Gottwein E.
903 2015. MicroRNA-Mediated Transformation by the Kaposi's Sarcoma-Associated
904 Herpesvirus Kaposin Locus. J Virol https://doi.org/10.1128/jvi.03317-14.

905 51. Corcoran JA, Johnston BP, McCormick C. 2015. Viral Activation of MK2-hsp27-
906 p115RhoGEF-RhoA Signaling Axis Causes Cytoskeletal Rearrangements, P-body
907 Disruption and ARE-mRNA Stabilization. PLoS Pathog
908 https://doi.org/10.1371/journal.ppat.1004597.

909 52. McCormick C, Ganem D. 2005. The kaposin B protein of KSHV activates the p38/MK2
910 pathway and stabilizes cytokine mRNAs. Science (80- )
911 https://doi.org/10.1126/science.1105779.

912 53. Corcoran JA, Khaperskyy DA, Johnston BP, King CA, Cyr DP, Olsthoorn A V.,
913 McCormick C. 2012. Kaposi's Sarcoma-Associated Herpesvirus G-Protein-Coupled
914 Receptor Prevents AU-Rich-Element-Mediated mRNA Decay. J Virol

915 https://doi.org/10.1128/jvi.00597-12.

916 54. Blanco FF, Sanduja S, Deane NG, Blackshear PJ, Dixon DA. 2014. Transforming Growth
917 Factor Regulates P-Body Formation through Induction of the mRNA Decay Factor
918 Tristetraprolin. Mol Cell Biol https://doi.org/10.1128/mcb.01020-13.

919 55. Franks TM, Lykke-Andersen J. 2007. TTP and BRF proteins nucleate processing body
920 formation to silence mRNAs with AU-rich elements. Genes Dev
921 https://doi.org/10.1101/gad.1494707.

922 56. Vindry C, Marnef A, Broomhead H, Twyffels L, Ozgur S, Stoecklin G, Llorian M, Smith
923 CW, Mata J, Weil D, Standart N. 2017. Dual RNA Processing Roles of Pat1b via
924 Cytoplasmic Lsm1-7 and Nuclear Lsm2-8 Complexes. Cell Rep
925 https://doi.org/10.1016/j.celrep.2017.06.091.

926 57. Hubstenberger A, Courel M, Bénard M, Souquere S, Ernoult-Lange M, Chouaib R, Yi Z,
927 Morlot JB, Munier A, Fradet M, Daunesse M, Bertrand E, Pierron G, Mozziconacci J,
928 Kress M, Weil D. 2017. P-Body Purification Reveals the Condensation of Repressed
929 mRNA Regulons. Mol Cell https://doi.org/10.1016/j.molcel.2017.09.003.

930 58. Brulois KF, Chang H, Lee AS-Y, Ensser A, Wong L-Y, Toth Z, Lee SH, Lee H-R,
931 Myoung J, Ganem D, Oh T-K, Kim JF, Gao S-J, Jung JU. 2012. Construction and
932 Manipulation of a New Kaposi's Sarcoma-Associated Herpesvirus Bacterial Artificial
933 Chromosome Clone. J Virol https://doi.org/10.1128/jvi.01019-12.

934 59. Myoung J, Ganem D. 2011. Generation of a doxycycline-inducible KSHV producer cell
935 line of endothelial origin: Maintenance of tight latency with efficient reactivation upon
936 induction. J Virol Methods https://doi.org/10.1016/j.jviromet.2011.03.012.

937 60. Kearse M, Moir R, Wilson A, Stones-Havas S, Cheung M, Sturrock S, Buxton S, Cooper
938 A, Markowitz S, Duran C, Thierer T, Ashton B, Meintjes P, Drummond A. 2012.
939 Geneious Basic: An integrated and extendable desktop software platform for the
940 organization and analysis of sequence data. Bioinformatics
941 https://doi.org/10.1093/bioinformatics/bts199.

942 61. Yoo SM, Ahn AK, Seo T, Hong HB, Chung MA, Jung SD, Cho H, Lee MS. 2008.
943 Centrifugal enhancement of Kaposi's sarcoma-associated virus infection of human
944 endothelial cells in vitro. J Virol Methods https://doi.org/10.1016/j.jviromet.2008.07.026.

945 62. Carpenter AE, Jones TR, Lamprecht MR, Clarke C, Kang IH, Friman O, Guertin DA,
946 Chang JH, Lindquist RA, Moffat J, Golland P, Sabatini DM. 2006. CellProfiler: Image
947 analysis software for identifying and quantifying cell phenotypes. Genome Biol
948 https://doi.org/10.1186/gb-2006-7-10-r100.

949 63. Castle E, Douglas P, Rinker K, Corcoran J. 2021. Viral manipulation of a novel
950 mechanoresponsive signaling axis disassembles processing bodies. bioRxiv
951 https://doi.org/10.1101/2020.05.15.091876.

952 64. Cannon JS, Ciufo D, Hawkins AL, Griffin CA, Borowitz MJ, Hayward GS, Ambinder RF.
953 2000. A New Primary Effusion Lymphoma-Derived Cell Line Yields a Highly Infectious
954 Kaposi's Sarcoma Herpesvirus-Containing Supernatant. J Virol
955 https://doi.org/10.1128/jvi.74.21.10187-10193.2000.

956 65. Tischer BK, Von Einem J, Kaufer B, Osterrieder N. 2006. Two-step Red-mediated
957 recombination for versatile high-efficiency markerless DNA manipulation in Escherichia
958 coli. Biotechniques https://doi.org/10.2144/000112096.

959 66. Santiago JC, Goldman JD, Zhao H, Pankow AP, Okuku F, Schmitt MW, Chen LH, Hill
960 CA, Casper C, Phipps WT, Mullins JI. 2021. Intra-host changes in Kaposi sarcoma-
961 associated herpesvirus genomes in Ugandan adults with Kaposi sarcoma. PLoS Pathog
962 https://doi.org/10.1371/journal.ppat.1008594.

963 67. BeltCappellino A, Majerciak V, Lobanov A, Lack J, Cam M, Zheng Z-M. 2019.
964 CRISPR/Cas9-Mediated Knockout and In Situ Inversion of the ORF57 Gene from All
965 Copies of the Kaposi's Sarcoma-Associated Herpesvirus Genome in BCBL-1 Cells . J
966 Virol https://doi.org/10.1128/jvi.00628-19.

967 68. Sallah N, Palser AL, Watson SJ, Labo N, Asiki G, Marshall V, Newton R, Whitby D,
968 Kellam P, Barroso I. 2018. Genome-wide sequence analysis of Kaposi sarcoma-associated
969 herpesvirus shows diversification driven by recombination. J Infect Dis
970 https://doi.org/10.1093/infdis/jiy427.

971 69. Tørresen OK, Star B, Mier P, Andrade-Navarro MA, Bateman A, Jarnot P, Gruca A,
972 Grynberg M, Kajava A V., Promponas VJ, Anisimova M, Jakobsen KS, Linke D. 2019.
973 Tandem repeats lead to sequence assembly errors and impose multi-level challenges for
974 genome and protein databases. Nucleic Acids Res.

975 70. Jain V, Plaisance-Bonstaff K, Sangani R, Lanier C, Dolce A, Hu J, Brulois K, Haecker I,
976 Turner P, Renne R, Krueger B. 2016. A toolbox for Herpesvirus miRNA research:
977 Construction of a complete set of KSHV miRNA Deletion Mutants. Viruses
978 https://doi.org/10.3390/V8020054.

979 71. Russo JJ, Bohenzky RA, Chien MC, Chen J, Yan M, Maddalena D, Parry JP, Peruzzi D,
980 Edelman IS, Chang Y, Moore PS. 1996. Nucleotide sequence of the Kaposi sarcoma-

981 associated herpesvirus (HHV8)Proceedings of the National Academy of Sciences of the
982 United States of America.

983 72. Dheekollu J, Chen H-S, Kaye KM, Lieberman PM. 2013. Timeless-Dependent DNA
984 Replication-Coupled Recombination Promotes Kaposi's Sarcoma-Associated Herpesvirus
985 Episome Maintenance and Terminal Repeat Stability. J Virol
986 https://doi.org/10.1128/jvi.02211-12.

987 73. Deutsch E, Cohen A, Kazimirsky G, Dovrat S, Rubinfeld H, Brodie C, Sarid R. 2004.
988 Role of Protein Kinase C δ in Reactivation of Kaposi's Sarcoma-Associated Herpesvirus.
989 J Virol https://doi.org/10.1128/jvi.78.18.10187-10192.2004.

990 74. Miller G, Rigsby MO, Heston L, Grogan E, Sun R, Metroka C, Levy JA, Gao S-J, Chang
991 Y, Moore P. 1996. Antibodies to Butyrate-Inducible Antigens of Kaposi's Sarcoma–
992 Associated Herpesvirus in Patients with HIV-1 Infection. N Engl J Med
993 https://doi.org/10.1056/nejm199605163342003.

994 75. Chen J, Ueda K, Sakakibara S, Okuno T, Parravicini C, Corbellino M, Yamanishi K.
995 2001. Activation of latent Kaposi's sarcoma-associated herpesvirus by demethylation of
996 the promoter of the lytic transactivator. Proc Natl Acad Sci U S A
997 https://doi.org/10.1073/pnas.051004198.

998 76. Renne R, Zhong W, Herndier B, McGrath M, Abbey N, Kedes D, Ganem D. 1996. Lytic
999 growth of Kaposi's sarcoma-associated herpesvirus (human herpesvirus 8) in culture. Nat
1000 Med https://doi.org/10.1038/nm0396-342.

1001 77. Haddad CO, Kalt I, Shovman Y, Xia L, Schlesinger Y, Sarid R, Parnas O. 2021. Targeting
1002 the Kaposi's sarcoma-associated herpesvirus genome with the CRISPR-Cas9 platform in

1003 latently infected cells. Virol J https://doi.org/10.1186/s12985-021-01527-x.

1004 78. Wen J, Zhao S, He D, Yang Y, Li Y, Zhu S. 2012. Preparation and characterization of egg
1005 yolk immunoglobulin Y specific to influenza B virus. Antiviral Res
1006 https://doi.org/10.1016/j.antiviral.2011.11.005.

1007 79. Brulois K, Toth Z, Wong L-Y, Feng P, Gao S-J, Ensser A, Jung JU. 2014. Kaposi's
1008 Sarcoma-Associated Herpesvirus K3 and K5 Ubiquitin E3 Ligases Have Stage-Specific
1009 Immune Evasion Roles during Lytic Replication. J Virol
1010 https://doi.org/10.1128/jvi.00873-14.

1011 80. Butnaru M, Gaglia MM. 2019. The kaposi's sarcoma-associated herpesvirus protein orf42
1012 is required for efficient virion production and expression of viral proteins. Viruses
1013 https://doi.org/10.3390/v11080711.

1014 81. Jiang HY, Yang WH, Gulick T, Bloch KD, Bloch DB. 2005. Ge-1 is a central component
1015 of the mammalian cytoplasmic mRNA processing body. RNA
1016 https://doi.org/10.1261/rna.2142405.

1017 82. Standart N, Weil D. 2018. P-Bodies: Cytosolic Droplets for Coordinated mRNA Storage.
1018 Trends Genet.

1019 83. Ciufo DM, Cannon JS, Poole LJ, Wu FY, Murray P, Ambinder RF, Hayward GS. 2001.
1020 Spindle Cell Conversion by Kaposi's Sarcoma-Associated Herpesvirus: Formation of
1021 Colonies and Plaques with Mixed Lytic and Latent Gene Expression in Infected Primary
1022 Dermal Microvascular Endothelial Cell Cultures. J Virol
1023 https://doi.org/10.1128/jvi.75.12.5614-5626.2001.

1024 84. Grossmann C, Podgrabinska S, Skobe M, Ganem D. 2006. Activation of NF-κB by the
1025 Latent vFLIP Gene of Kaposi's Sarcoma-Associated Herpesvirus Is Required for the
1026 Spindle Shape of Virus-Infected Endothelial Cells and Contributes to Their
1027 Proinflammatory Phenotype. J Virol https://doi.org/10.1128/jvi.01603-05.

1028 85. Alkharsah KR, Singh V V., Bosco R, Santag S, Grundhoff A, Konrad A, Sturzl M, Wirth
1029 D, Dittrich-Breiholz O, Kracht M, Schulz TF. 2011. Deletion of Kaposi's Sarcoma-
1030 Associated Herpesvirus FLICE Inhibitory Protein, vFLIP, from the Viral Genome
1031 Compromises the Activation of STAT1-Responsive Cellular Genes and Spindle Cell
1032 Formation in Endothelial Cells. J Virol https://doi.org/10.1128/jvi.00226-11.

1033 86. Yoo J, Kang J, Lee HN, Aguilar B, Kafka D, Lee S, Choi I, Lee J, Ramu S, Haas J, Koh
1034 CJ, Hong YK. 2010. Kaposin-B enhances the PROX1 mRNA stability during lymphatic
1035 reprogramming of vascular endothelial cells by Kaposi's sarcoma herpes virus. PLoS
1036 Pathog https://doi.org/10.1371/journal.ppat.1001046.

1037 87. Chang HC, Hsieh TH, Lee YW, Tsai CF, Tsai YN, Cheng CC, Wang HW. 2016. c-Myc
1038 and viral cofactor Kaposin B co-operate to elicit angiogenesis through modulating
1039 miRNome traits of endothelial cells. BMC Syst Biol https://doi.org/10.1186/s12918-015-
1040 0242-3.

1041 88. Aguilar B, Choi I, Choi D, Chung HK, Lee S, Yoo J, Lee YS, Maeng YS, Lee HN, Park
1042 E, Kim KE, Kim NY, Baik JM, Jung JU, Koh CJ, Hong YK. 2012. Lymphatic
1043 reprogramming by Kaposi sarcoma herpes virus promotes the oncogenic activity of the
1044 virus-encoded G-protein-coupled receptor. Cancer Res https://doi.org/10.1158/0008-
1045 5472.CAN-12-1229.

1046 89. Toth Z, Papp B, Brulois K, Choi YJ, Gao SJ, Jung JU. 2016. LANA-Mediated
1047 Recruitment of Host Polycomb Repressive Complexes onto the KSHV Genome during De
1048 Novo Infection. PLoS Pathog https://doi.org/10.1371/journal.ppat.1005878.

1049 90. Gallo A, Lampe M, Günther T, Brune W. 2017. The Viral Bcl-2 Homologs of Kaposi's
1050 Sarcoma-Associated Herpesvirus and Rhesus Rhadinovirus Share an Essential Role for
1051 Viral Replication. J Virol https://doi.org/10.1128/jvi.01875-16.

1052 91. Campbell M, Watanabe T, Nakano K, Davis RR, Lyu Y, Tepper CG, Durbin-Johnson B,
1053 Fujimuro M, Izumiya Y. 2018. KSHV episomes reveal dynamic chromatin loop formation
1054 with domain-specific gene regulation. Nat Commun https://doi.org/10.1038/s41467-017-
1055 02089-9.

1056 92. West JA, Wicks M, Gregory SM, Chugh P, Jacobs SR, Zhang Z, Host KM, Dittmer DP,
1057 Damania B. 2014. An Important Role for Mitochondrial Antiviral Signaling Protein in the
1058 Kaposi's Sarcoma-Associated Herpesvirus Life Cycle. J Virol
1059 https://doi.org/10.1128/jvi.03226-13.

1060 93. Barbera AJ, Chodaparambil J V., Kelley-Clarke B, Joukov V, Walter JC, Luger K, Kaye
1061 KM. 2006. The nucleosomal surface as a docking station for Kaposi's sarcoma
1062 herpesvirus LANA. Science (80- ) https://doi.org/10.1126/science.1120541.

1063 94. Hellert J, Weidner-Glunde M, Krausze J, Richter U, Adler H, Fedorov R, Pietrek M,
1064 Rückert J, Ritter C, Schulz TF, Lührs T. 2013. A Structural Basis for BRD2/4-Mediated
1065 Host Chromatin Interaction and Oligomer Assembly of Kaposi Sarcoma-Associated
1066 Herpesvirus and Murine Gammaherpesvirus LANA Proteins. PLoS Pathog
1067 https://doi.org/10.1371/journal.ppat.1003640.

1068 95. Vladimirova O, de Leo A, Deng Z, Wiedmer A, Hayden J, Lieberman PM. 2021. Phase
1069 separation and DAXX redistribution contribute to LANA nuclear body and KSHV
1070 genome dynamics during latency and reactivation. PLoS Pathog
1071 https://doi.org/10.1371/journal.ppat.1009231.

1072 96. Lin CL, Li H, Wang Y, Zhu FX, Kudchodkar S, Yuan Y. 2003. Kaposi's Sarcoma-
1073 Associated Herpesvirus Lytic Origin (ori-Lyt)-Dependent DNA Replication: Identification
1074 of the ori-Lyt and Association of K8 bZip Protein with the Origin. J Virol
1075 https://doi.org/10.1128/jvi.77.10.5578-5588.2003.

1076 97. Wang Y, Li H, Chan MY, Zhu FX, Lukac DM, Yuan Y. 2004. Kaposi's Sarcoma-
1077 Associated Herpesvirus ori-Lyt-Dependent DNA Replication: cis-Acting Requirements
1078 for Replication and ori-Lyt-Associated RNA Transcription. J Virol
1079 https://doi.org/10.1128/jvi.78.16.8615-8629.2004.

1080 98. Wang Y, Tang Q, Maul GG, Yuan Y. 2006. Kaposi's Sarcoma-Associated Herpesvirus
1081 ori-Lyt-Dependent DNA Replication: DualRole of Replication and Transcription
1082 Activator. J Virol https://doi.org/10.1128/jvi.00990-06.

1083 99. Liu D, Wang Y, Yuan Y. 2018. Kaposi's Sarcoma-Associated Herpesvirus K8 Is an RNA
1084 Binding Protein That Regulates Viral DNA Replication in Coordination with a Noncoding
1085 RNA. J Virol https://doi.org/10.1128/jvi.02177-17.

1086 100. Sharma NR, Majerciak V, Kruhlak MJ, Yu L, Kang JG, Yang A, Gu S, Fritzler MJ, Zheng
1087 ZM. 2019. KSHV RNA-binding protein ORF57 inhibits P-body formation to promote
1088 viral multiplication by interaction with Ago2 and GW182. Nucleic Acids Res
1089 https://doi.org/10.1093/nar/gkz683.

1090 101. Wang X, Chang L, Wang H, Su A, Wu Z. 2017. Dcp1a and GW182 Induce Distinct
1091 Cellular Aggregates and Have Different Effects on microRNA Pathway. DNA Cell Biol
1092 https://doi.org/10.1089/dna.2017.3633.

1093

1094

1095 **Table 1: BAC16 Mutagenesis Primers**

| **Primer**<br>*Fwd. is forward primer*<br>*Rev. is reverse primer* | **Sequence**<br>*Restriction enzyme recognition sites are bolded*<br>*BAC16 homology regions are underlined*<br>*Complementary target sequences are italicized.* |
|---|---|
| KanSacB Homology – Fwd. | 5' ATACAT**GGATCC***AGGATGACGACGATAA GTAGGGATAACAGGGTAAT* 3' |
| KanSacB Homology – Rev. | 5' ATTAGT**GCGGCCGC**<u>GGACATGAACTGCC ACAAACACCGTTAAGCCTCTATCCAT</u>*CAACCAAT TAACCAATTCTGAT* 3' |
| altKapC Homology – Fwd. | 5' ATACAT**GCTAGC**<u>CGGAGGACGGATCTCT TGGATTTACACGTATCGAGGAGCG</u>*GTAGCACCC CAGGAACCCGTCCTAGCACACCCCA* 3' |
| altKapC Homology – Rev. | 5' TGATTA**GGATCC**<u>GGACATGAACTGCCAC AAACACCGTTAAGCCTCTATCCAT</u>A*CACTGAGAT TGAAGAG* 3' |
| altKapB Homology – Fwd. | 5' ATACAT**GCTAGC**<u>CGGAGGACGGATCTCT TGGATTTACACGTATCGAGGAGCG</u>*GTGGCACCC CAGGAACCCGT* 3' |
| altKapB Homology – Rev. | 5' TGATTA**GGATCC**<u>GGACATGAACTGCCAC AAACACCGTTAAGCCTCTATCCAT</u>*GCATAGGTAT AGGTGGTAGA* 3' |
| Kaposin Screening – Fwd. | 5' <u>*CAGGAAACGCTATAAAGAAGAGG*</u> 3' |

| | |
|---|---|
| Kaposin Screening – Rev. | 5’ *ACAGACAAACGAGTGGTGGTATC* 3’ |
| altKapC Screening – Rev. | 5’ *ATTACCTGGAAGCAATGCACC* 3’ |
| altKapB Screening – Rev. | 5’ *TGATGAAGGAACTAGATTGCCAG* 3’ |
| KanSacB Screening – Fwd. | 5’ *GCGACAACCATACGCTGAGAG* 3’ |
| Revertant Screening – Rev. (Homology primer) | 5’ *ACACCGTTAAGCCTCTATCCAT* 3’ |
| Revertant Screening – Rev. (Revert primer) | 5’ *TGCATTGGGATTGGAGTGAGGA* 3’ |

1096

1097

1098

1099

1100

1101

1102

1103

1104

1105

1106

1107

1108

1109 **Table 2: Antibodies**

| Antibody | Species | Vendor/Catalogue # | Application | Dilution |
|---|---|---|---|---|
| Hedls | Mouse | Santa-Cruz sc-8418 | Immunofluorescence | 1:1000 |
| KapB | Rabbit | A generous gift from Don Ganem | Immunoblot | 1:1000 |
| LANA | Rabbit | A generous gift from Don Ganem | Immunofluorescence<br>Immunoblot | 1:1000<br>1:1000 |
| Alexa Fluor™ 647 Phalloidin | N/A | Thermo Fisher A22287 | Immunofluorescence | 1:100 |
| Alexa Fluor™ 488 | Chicken anti-Rabbit | Thermo Fisher A-21441 | Immunofluorescence | 1:1000 |
| Alexa Fluor™ 647 | Chicken anti-Mouse | Thermo Fisher A-21463 | Immunofluorescence | 1:1000 |
| Hoechst 33342 | N/A | Thermo Fisher H3570 | Immunofluorescence | 1:10000 |
| Beta-Actin HRP Conjugate | Rabbit | Cell Signaling Technologies 5125 | Immunoblot | 1:8000 |
| Anti-rabbit IgG HRP-linked | N/A | Cell Signaling Technologies 7074 | Immunoblot | 1:3000 |

1110

1111

1112

1113

1114

1115

1116 **Table 3: qPCR primers**

| Primer | Sequence |
|---|---|
| qPCR ORF26 – Forward | 5’ CAGTTGAGCGTCCCAGATGA 3’ |
| qPCR ORF26 – Reverse | 5’ GGAATACCAACAGGAGGCCG 3’ |
| qPCR β-actin – Forward | 5’ CTTCCAGCAGATGTGGATCA 3’ |
| qPCR β-actin – Reverse | 5’ AAAGCCATGCCAATCTCATC 3’ |
| qPCR Luc – Forward | 5’ TGCGCAAGAATAGCTCCTCC 3’ |
| qPCR Luc – Reverse | 5’ TTCGGCAACCAGATCATCCC 3’ |

1117

1118

1119

1120

1121

1122

1123

1124

1125

1126

1127

1128

1129

1130

1131 **Figure Legends**

1132 **Figure 1. Lambda Red recombination facilitates the creation of five kaposin-deficient**
1133 **BAC16 DNA constructs. (A)** A simplified version of the kaposin transcript is depicted in the 5'
1134 to 3' orientation. Open reading frames for kaposin A (KapA), kaposin B (KapB), and kaposin C
1135 (KapC) are indicated with corresponding AUG, GUG and CUG start codons for each. DR1 =
1136 direct repeat 1, DR2 = direct repeat 2, K12 = the KapA ORF. **(B)** An example of the re-coding
1137 strategy used to create the BAC16ΔKapB virus construct is shown. Wildtype nucleotide and
1138 corresponding amino acid repeats are show above with recoded nucleotides (red) and
1139 corresponding amino acid changes depicted below. **(C)** The Lambda Red recombination method
1140 used to create all kaposin-deficient BAC16 viruses is shown; the strategy for BAC16ΔKapB is
1141 depicted as an example. **(D)** Each kaposin-deficient BAC16 construct is shown relative to that of
1142 the wildtype *kaposin* locus in its genomic position (only reverse strand is shown for simplicity).

1143

1144 **Figure 2. Confirmation of the panel BAC16 kaposin-deficient viruses. (A)** BAC16 DNA was
1145 isolated from GS1783 *E.coli* harbouring recombinant or WT BAC16 DNA and then subjected to
1146 whole genome sequencing (WGS). Raw reads were paired, trimmed, and mapped to the BAC16
1147 genome (NCBI accession #GQ994935) in Geneious Prime. Coverage for each recombinant is
1148 indicated in blue with an average coverage per nucleotide of between 670-1430x. BAC16 ORFs
1149 are depicted in turquoise, repeat regions in orange and the *kaposin* locus is outlined in red.
1150 Variants were detected based on a minimum coverage of 5 and minimum frequency variation of
1151 0.25 and are depicted in magenta. **(B)** Representative zoom panels of read alignment to the
1152 *kaposin* locus of WT and ΔKapB are shown. **(C)** BAC16 DNA was isolated from GS1783 *E.coli*
1153 and digested using NheI and fragments were subjected to pulsed-field gel electrophoresis

1154 (PFGE). Based on *in silco* predictions, *kaposin* locus containing fragments are indicated with a
1155 red asterisk.

1156

1157 **Figure 3. Generation of stable latent kaposin-deficient BAC16 iSLK cell lines by co-culture**
1158 **method. (A-D)** 293T cells were transfected with recombinant or WT BAC16 DNA. 48 hours
1159 post transfection, cells were selected with hygromycin (increasing concentration from 50 µg/mL
1160 to 100 µg/mL) until a confluent layer of BAC16-containing 293T cells was achieved. **(B)** Images
1161 of BAC16-293Ts were captured using an EVOS-FL microscope with the 10X objective. **(C)**
1162 Latent BAC16-293T cells were trypsinzed, pelleted and lysed to extract DNA. qPCR was
1163 preformed using ORF26 and β-actin specific primers. Values are represented as fold change
1164 relative WT. *n*=3; mean ± SD. **(D-F)** BAC16-293Ts were seeded in a 2:1 ratio with naïve iSLK
1165 cells. Cells were treated with 1 mM NaB and 20 ng/mL TPA for 96 hours, virus-containing
1166 supernatant was removed and replaced with media containing puromycin (10 µg/mL) and
1167 hygromycin (increasing concentration from 200 µg/mL to 1200 µg/mL) until a confluent layer of
1168 BAC16-containing iSLK cells was achieved **(E).** Latent iSLKs were fixed, permeabilized and
1169 immunostained using antisera for viral LANA (green) to visualize infected nuclei and Hoescht to
1170 visualize total cell nuclei (blue)**.** Images were captured using Zeiss AxioObserver Z1 microscope
1171 with the 40X objective. Scale bar = 20 µm. **(F)** BAC16-containing iSLKs were trypsinized,
1172 pelleted and lysed to extract DNA. qPCR was performed using ORF26 and β-actin specific
1173 primers. Values are represented as fold change relative to WT. *n*=3; mean ± SD, (*, $P < 0.05$; **,
1174 $P < 0.01$; ***, $P < 0.001$; ns, nonsignificant).

1175

1176 **Figure 4. Removal of kaposin direct repeats accelerates KSHV episome loss from latent**
1177 **iSLK cells.** Latent iSLK cells were serially passaged in the absence of hygromycin for a total of
1178 14 passages. At each passage, a sample of cells was taken, pelleted and used for DNA extraction.
1179 To quantify levels of viral DNA, qPCR was performed using viral ORF26 and host β-actin
1180 specific primers. **(A)** Values are represented as fold change relative to genome copy number in
1181 wild-type (WT) BAC16 iSLK cells at passages 1 (P1) $n = 3$; means ± SD, **(***, $P < 0.05$; **, $P <$
1182 $0.01$; ***, $P < 0.001$; ns, nonsignificant). **(B)** Values are represented as fold change relative to
1183 the corresponding starting passage (P1), for each recombinant virus over the course of the
1184 experiment. $n = 3$; mean ± SD. The red line was obtained using linear regression analysis and the
1185 slope of the line is depicted in the top right corner for each graph.

1186

1187 **Figure 5. Kaposin-deficient BAC16 iSLK cells produce progeny virions when reactivated.**
1188 **(A)** BAC16-iSLK cells were reactivated using 1 μg/mL Dox for 24 hours prior to lysis and
1189 immunoblotting using antisera that recognizes DR1 in both KapB and KapC. Specific antibody
1190 to β-actin served as a loading control. One representative experiment of three is shown. **(B-C)**
1191 BAC16-iSLK cells were reactivated with 1 μg/mL Dox and 1 mM NaB for 0, 24, 48, 72, or 96
1192 hours. At each time point cells were trypsinized, pelleted and lysed to extract DNA. qPCR was
1193 performed using ORF26 and host β-actin specific primers. Values represent either fold-change
1194 relative to time 0 (latency) for each recombinant virus (B) $n$=3, mean ± SD, or fold-change
1195 relative to WT at 0, 24, 48, 72 and 96 hours post reactivation, (C) $n$=3; mean ± SD**,** (*, $P < 0.05$;
1196 **, $P < 0.01$; ***, $P < 0.001$; ns, nonsignificant). **(D).** BAC16-iSLK cells were reactivated as
1197 above for 96 hours, virus-containing supernatant was collected, clarified and DNase-treated prior
1198 to extraction of virion-protected DNA. qPCR was performed using ORF26 and luciferase

1199 (control) specific primers. Values represented fold-change relative to WT. *n*=3; mean ± SD, (*, P
1200 < 0.05; **, P < 0.01; ***, P < 0.001; ns, nonsignificant). **(E)** BAC16-iSLK cells were reactivated
1201 for 96 hours. Virus-containing supernatant for each recombinant cell line was then collected,
1202 clarified, and diluted 1:4 with fresh DMEM and used to infect naïve 293T cells. After 24h, cells
1203 were fixed, permeabilized and stained using antisera specific for viral LANA (green) and
1204 Hoescht (nucleus, blue)**.** Images were captured using Zeiss AxioObserver Z1 microscope with
1205 the 40X objective. Scale bar = 20 μm. One representative experiment is shown.

1206

1207 **Figure 6. Primary infection of endothelial cells with BAC16ΔKapB virus is impaired.**

1208 **(A-B)** Equal numbers of virus particles (based on DNase-protected extracellular genome copy
1209 number) of WT and either ΔKapB-1 and ΔKapB-2 were used to infect HUVECs. 24h later, cells
1210 were fixed, permeabilized and immunstained for viral LANA, then stained with Hoescht. The
1211 number of LANA-expressing cells was quantified and is represented as a percent of the total
1212 number of cells counted. *n*=2; mean ± SD. **(C)** Images of four different ΔKapB BAC16-iSLK
1213 latent cell lines and WT BAC16-iSLKs were captured using an EVOS-FL microscope with the
1214 10X objective. One representative experiment of two is shown. **(D-F)** Latent ΔKapB and WT
1215 BAC16-iSLKs were fixed, permeabilized and immunostained for viral LANA, then stained with
1216 Hoescht. LANA-NBs were visualized (D), and the number of LANA-NBs per cell was counted
1217 using CellProfiler (E) *n*=2; mean ± SD. LANA-NB area was calcuated for at approximently 4000
1218 individual LANA-NBs per cell line and the distribution of area shown in (F). **(G)** Latent ΔKapB
1219 and WT BAC16-iSLKs were trypsinized, pelleted and lysed to extract DNA. qPCR was
1220 preformed using ORF26 and β-actin specific primers. Values are represented as fold change
1221 relative WT. *n*=3, mean ± SD**,** (*, P < 0.05; **, P < 0.01; ***, P < 0.001; ns, nonsignificant). **(H)**

1222 Latent BAC16-iSLKs were lysed and harvested for immunoblotting using LANA and β-actin
1223 specific antibodies. One representative experiment of two is shown.

1224

1225 **Figure 7. KapB is required for PB disassembly following *de novo* HUVEC infection. (A)**
1226 WT and ΔKapB BAC16 viruses were titrated using 293T cells and RFP expression was used to
1227 estimate an equal number of infectious virions for subsequent *de novo* infection of HUVECs. At
1228 96hpi, HUVECs were fixed, permeabilized and immunostained for either viral LANA (green),
1229 the PB-resident protein Hedls/EDC4 (white) then stained with Hoescht (nucleus, blue). Images
1230 were captured using Zeiss AxioObserver Z1 microscope with the 40X objective. Scale bar = 20
1231 µm. **(B)** Hedls puncta per cell were quantified using CellProfiler. For mock infections, all cells
1232 were counted; for WT and ΔKapB-infected cells, only LANA-positive cells were counted. Data
1233 is represented as fold change in PBs per cell relative to mock infection. A repeated measures
1234 one-way ANOVA was performed. $n$=4; mean ± SD, (*, $P < 0.05$; **, $P < 0.01$; ***, $P < 0.001$;
1235 ns, nonsignificant). **(C)** Cells infected as in (A) were lysed at 96 hpi and harvested for
1236 immunoblotting using LANA, DR1 (KapB and C) and β-actin specific antibodies. One
1237 representative experiment of three is shown. **(D)** WT and ΔKapB BAC16 viruses were titrated as
1238 in (A) prior to infecting HUVECs. At 96 hpi, brightfield images were acquired at 10X, cells were
1239 fixed, permeabilized and immunostained for viral LANA (green). Phalloidin and Hoescht
1240 staining was used to visualize actin (white) and nuclei (blue), respectively. Images were captured
1241 using Zeiss AxioObserver Z1 microscope with the 40X objective. Scale bar = 20 µm. One
1242 representative image of three experiments is shown.

Figure 1

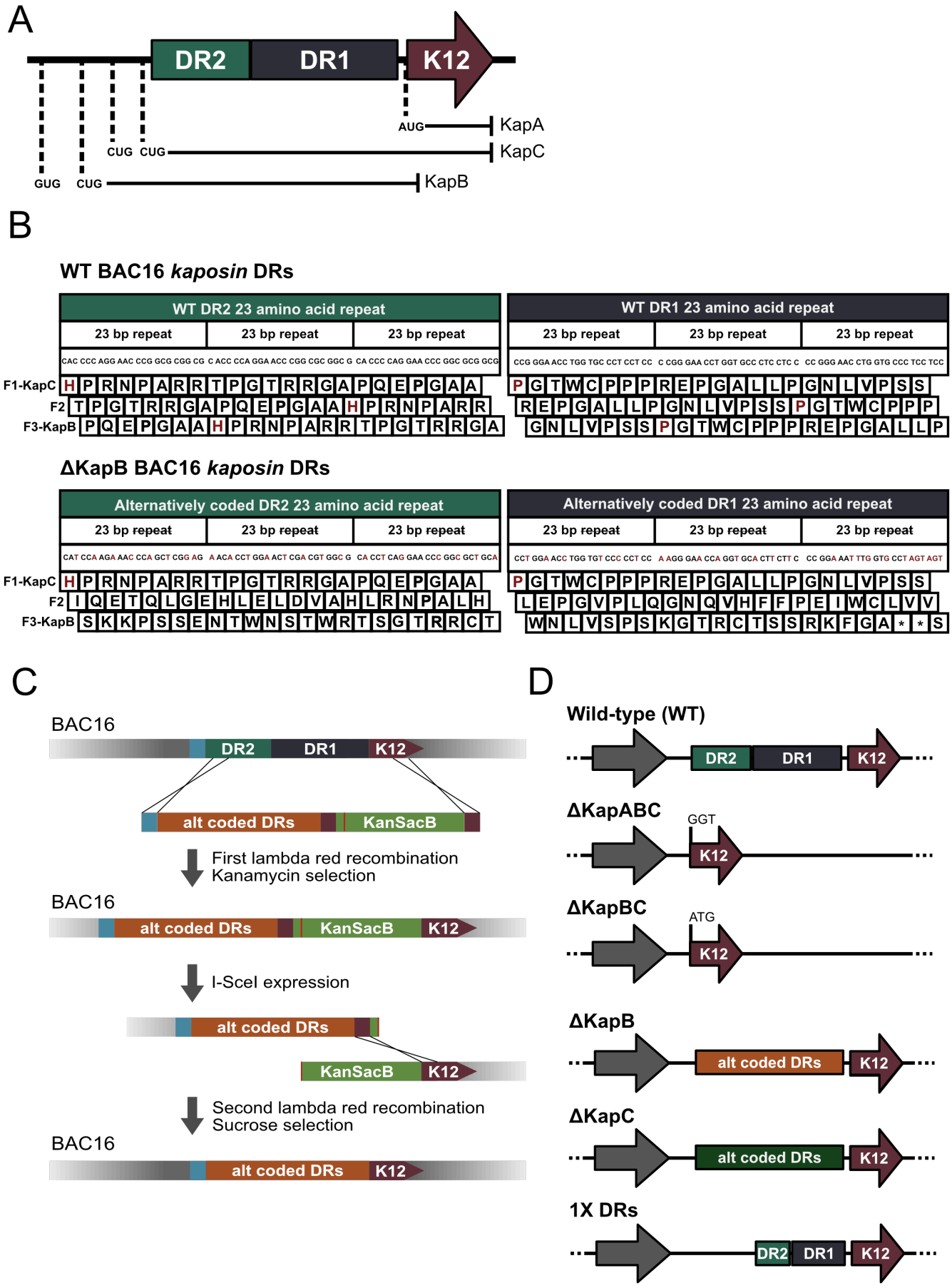
A
DR2
DR1
K12
AUG
KapA
CUG CUG
KapC
GUG CUG
KapB
B
WT BAC16 kaposin DRs
WT DR2 23 amino acid repeat
23 bp repeat
23 bp repeat
23 bp repeat
CAC CCC AGG AAC CCG GCG CGG CG C ACC CCA GGA ACC CGG CGC GGC G CA CCC CAG GAA CCC GGC GCG GCG
F1-KapC H P R N P A R R T P G T R R G A P Q E P G A A
F2 T P G T R R G A P Q E P G A A H P R N P A R R
F3-KapB P Q E P G A A H P R N P A R R T P G T R R G A
WT DR1 23 amino acid repeat
23 bp repeat
23 bp repeat
23 bp repeat
CCG GGA ACC TGG TGC CCT CCT CC C CGG GAA CCT GGT GCC CTC CTC C CC GGG AAC CTG GTG CCC TCC TCC
P G T W C P P P R E P G A L L P G N L V P S S
R E P G A L L P G N L V P S S P G T W C P P P
G N L V P S S P G T W C P P P R E P G A L L P
ΔKapB BAC16 kaposin DRs
Alternatively coded DR2 23 amino acid repeat
23 bp repeat
23 bp repeat
23 bp repeat
CAT CCA AGA AAC CCA GCT CGG AG A ACA CCT GGA ACT CGA CGT GGC G CA CCT CAG GAA CCC GGC GCT GCA
F1-KapC H P R N P A R R T P G T R R G A P Q E P G A A
F2 I Q E T Q L G E H L E L D V A H L R N P A L H
F3-KapB S K K P S S E N T W N S T W R T S G T R R C T
Alternatively coded DR1 23 amino acid repeat
23 bp repeat
23 bp repeat
23 bp repeat
CCT GGA ACC TGG TGT CCC CCT CC A AGG GAA CCA GGT GCA CTT CTT C CC GGA AAT TTG GTG CCT AGT AGT
P G T W C P P P R E P G A L L P G N L V P S S
L E P G V P L Q G N Q V H F F P E I W C L V V
W N L V S P S K G T R C T S S R K F G A * * S
C
BAC16
DR2
DR1
K12
alt coded DRs
KanSacB
First lambda red recombination
Kanamycin selection
BAC16
alt coded DRs
KanSacB
K12
I-SceI expression
alt coded DRs
KanSacB
K12
Second lambda red recombination
Sucrose selection
BAC16
alt coded DRs
K12
D
Wild-type (WT)
DR2
DR1
K12
ΔKapABC
GGT
K12
ΔKapBC
ATG
K12
ΔKapB
alt coded DRs
K12
ΔKapC
alt coded DRs
K12
1X DRs
DR2
DR1
K12

Figure 2

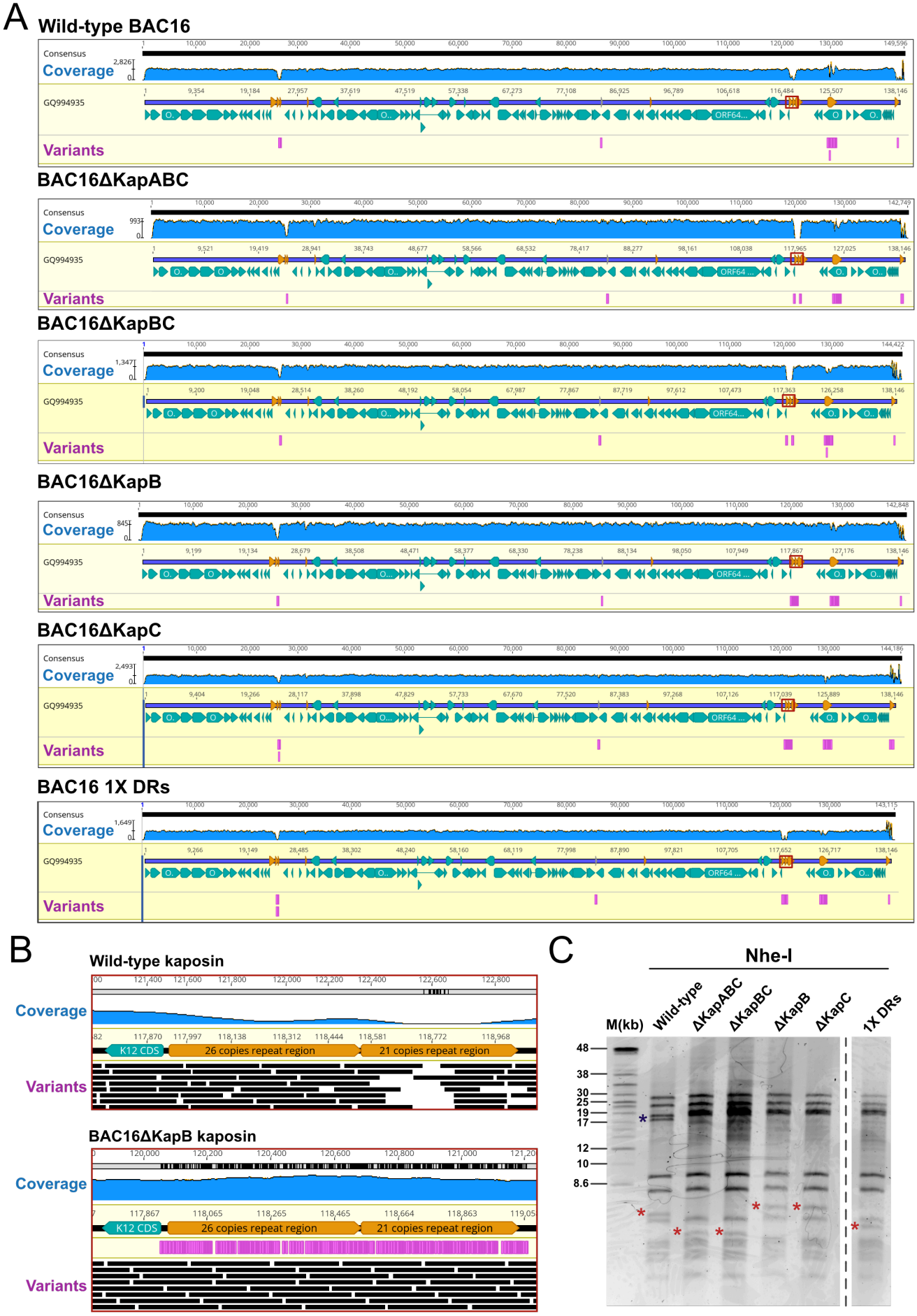
A
Wild-type BAC16
BAC16ΔKapABC
BAC16ΔKapBC
BAC16ΔKapB
BAC16ΔKapC
BAC16 1X DRs
Consensus
Coverage
GQ994935
Variants
ORF64...
B
Wild-type kaposin
Coverage
K12 CDS
26 copies repeat region
21 copies repeat region
Variants
BAC16ΔKapB kaposin
Coverage
K12 CDS
26 copies repeat region
21 copies repeat region
Variants
C
Nhe-I
M(kb)
Wild-type
ΔKapABC
ΔKapBC
ΔKapB
ΔKapC
1X DRs
48
38
30
25
19
17
12
10
8.6

Figure 3

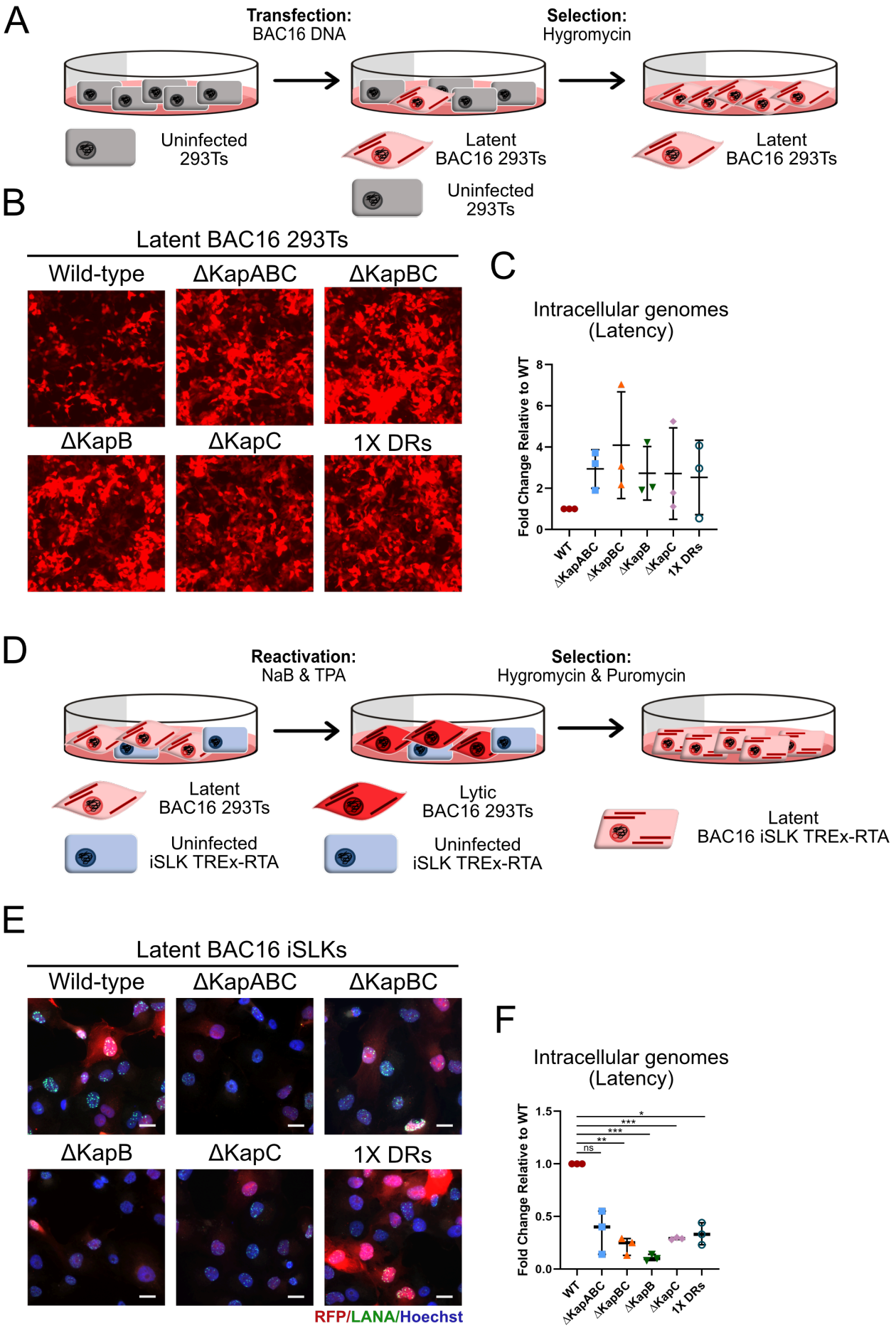
A
Transfection:
BAC16 DNA
Selection:
Hygromycin
Uninfected
293Ts
Latent
BAC16 293Ts
Uninfected
293Ts
Latent
BAC16 293Ts
B
Latent BAC16 293Ts
Wild-type
ΔKapABC
ΔKapBC
ΔKapB
ΔKapC
1X DRs
C
Intracellular genomes
(Latency)
Fold Change Relative to WT
0
2
4
6
8
WT
ΔKapABC
ΔKapBC
ΔKapB
ΔKapC
1X DRs
D
Reactivation:
NaB & TPA
Selection:
Hygromycin & Puromycin
Latent
BAC16 293Ts
Uninfected
iSLK TREx-RTA
Lytic
BAC16 293Ts
Uninfected
iSLK TREx-RTA
Latent
BAC16 iSLK TREx-RTA
E
Latent BAC16 iSLKs
Wild-type
ΔKapABC
ΔKapBC
ΔKapB
ΔKapC
1X DRs
RFP/LANA/Hoechst
F
Intracellular genomes
(Latency)
Fold Change Relative to WT
0.0
0.5
1.0
1.5
ns
**
***
***
*
WT
ΔKapABC
ΔKapBC
ΔKapB
ΔKapC
1X DRs

Figure 4

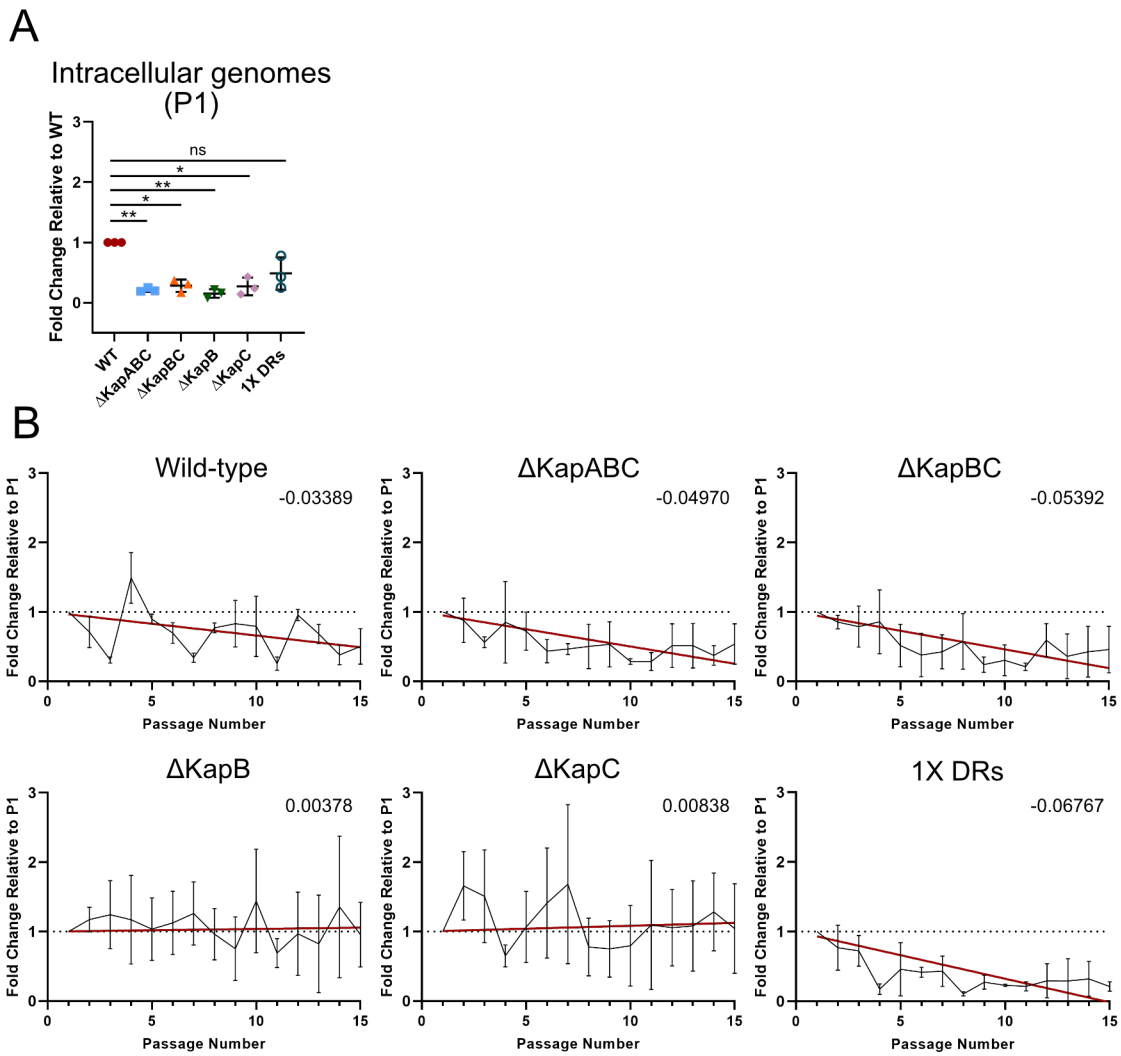
A
Intracellular genomes
(P1)
Fold Change Relative to WT
ns
*
**
*
**
WT
ΔKapABC
ΔKapBC
ΔKapB
ΔKapC
1X DRs
B
Wild-type
-0.03389
ΔKapABC
-0.04970
ΔKapBC
-0.05392
ΔKapB
0.00378
ΔKapC
0.00838
1X DRs
-0.06767
Fold Change Relative to P1
Passage Number

Figure 5

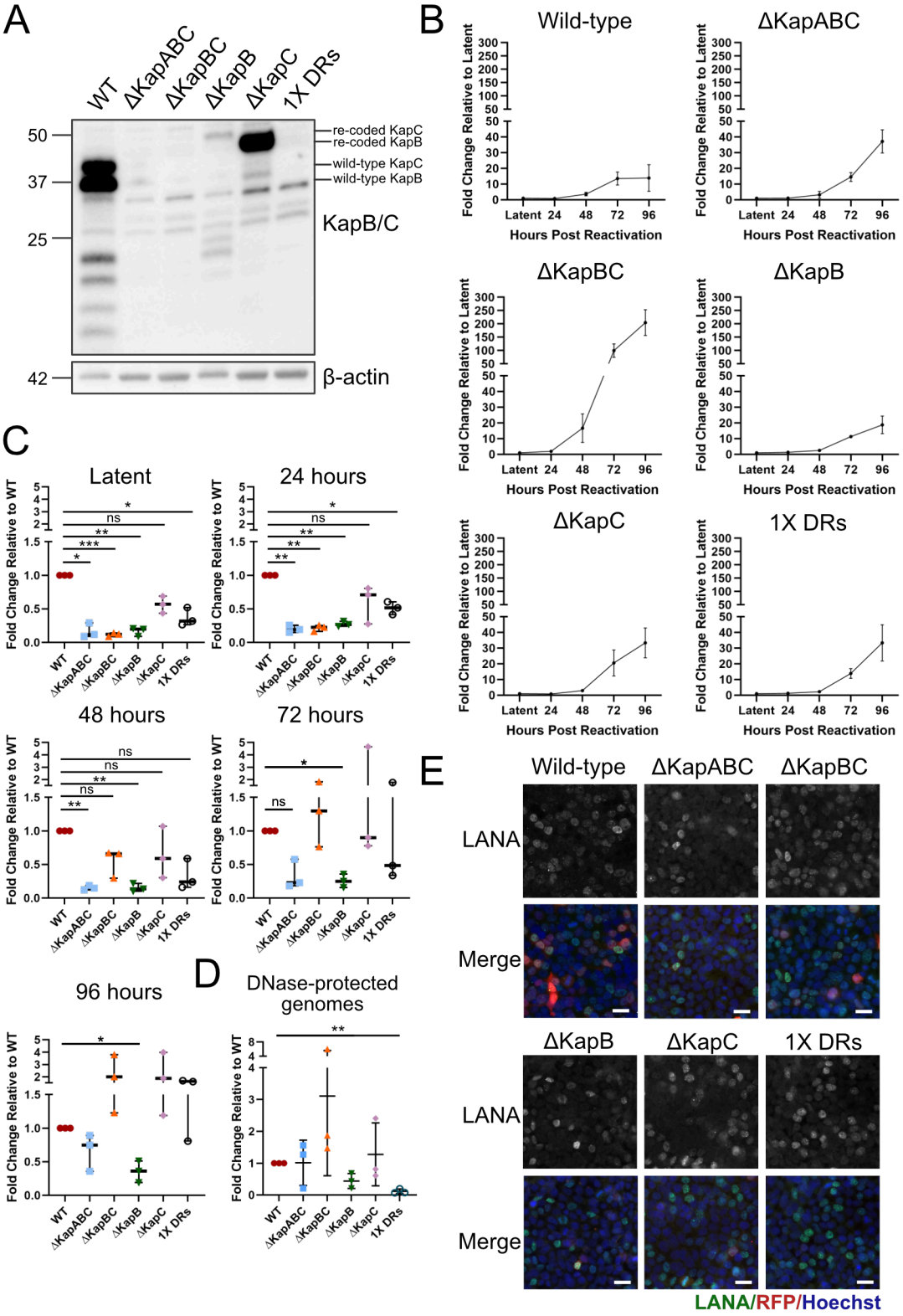
A
WT
ΔKapABC
ΔKapBC
ΔKapB
ΔKapC
1X DRs
50
37
25
42
re-coded KapC
re-coded KapB
wild-type KapC
wild-type KapB
KapB/C
β-actin
B
Wild-type
ΔKapABC
ΔKapBC
ΔKapB
ΔKapC
1X DRs
Fold Change Relative to Latent
Latent 24 48 72 96
Hours Post Reactivation
C
Latent
24 hours
48 hours
72 hours
96 hours
Fold Change Relative to WT
WT
ΔKapABC
ΔKapBC
ΔKapB
ΔKapC
1X DRs
D
DNase-protected genomes
E
Wild-type
ΔKapABC
ΔKapBC
ΔKapB
ΔKapC
1X DRs
LANA
Merge
LANA/RFP/Hoechst

Figure 6

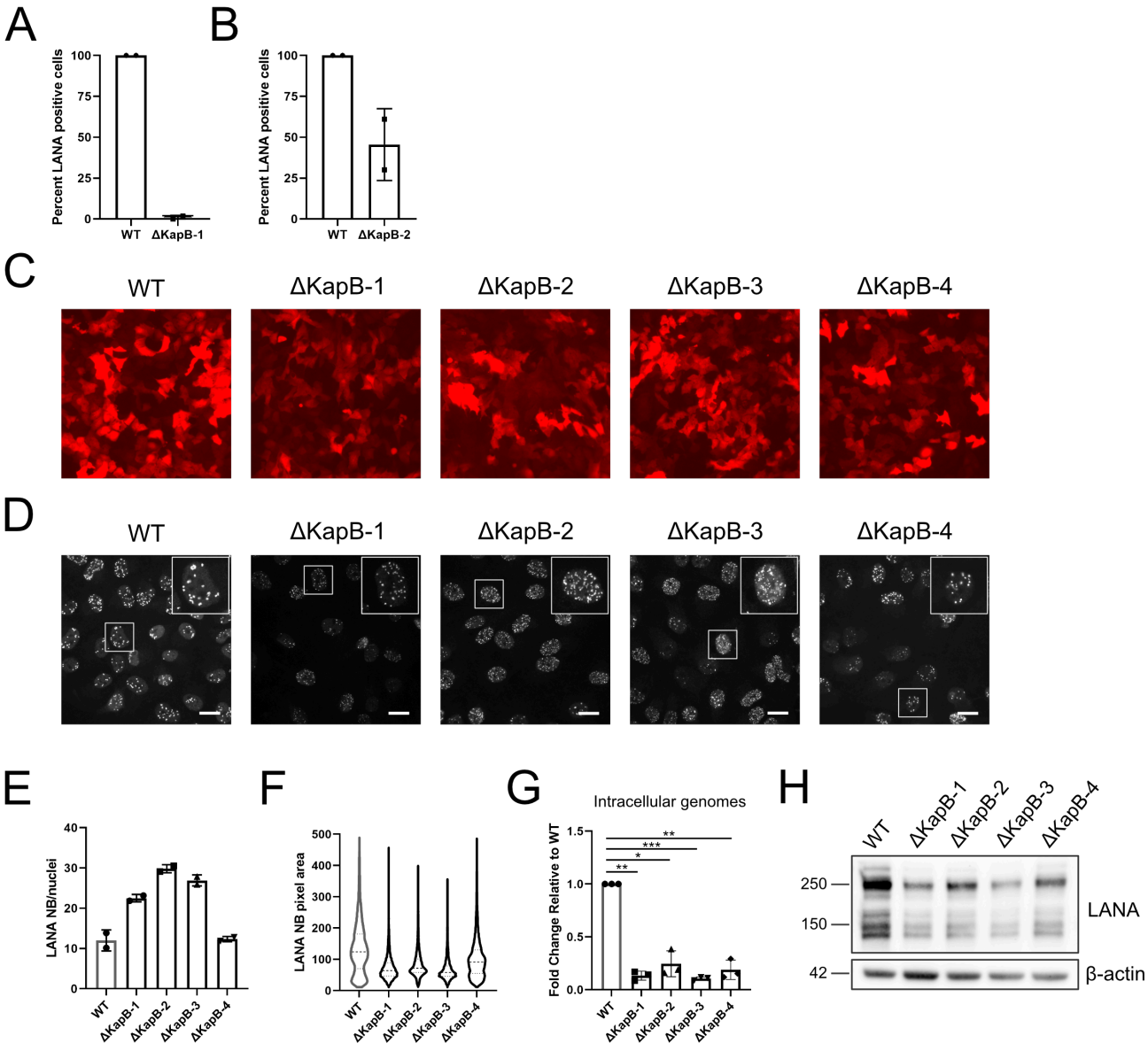
A
Percent LANA positive cells
100
75
50
25
0
WT
ΔKapB-1
B
Percent LANA positive cells
100
75
50
25
0
WT
ΔKapB-2
C
WT
ΔKapB-1
ΔKapB-2
ΔKapB-3
ΔKapB-4
D
WT
ΔKapB-1
ΔKapB-2
ΔKapB-3
ΔKapB-4
E
LANA NB/nuclei
40
30
20
10
0
WT
ΔKapB-1
ΔKapB-2
ΔKapB-3
ΔKapB-4
F
LANA NB pixel area
500
400
300
200
100
0
WT
ΔKapB-1
ΔKapB-2
ΔKapB-3
ΔKapB-4
G
Intracellular genomes
Fold Change Relative to WT
1.5
1.0
0.5
0.0
**
***
*
**
WT
ΔKapB-1
ΔKapB-2
ΔKapB-3
ΔKapB-4
H
WT
ΔKapB-1
ΔKapB-2
ΔKapB-3
ΔKapB-4
250
150
42
LANA
β-actin

Figure 7

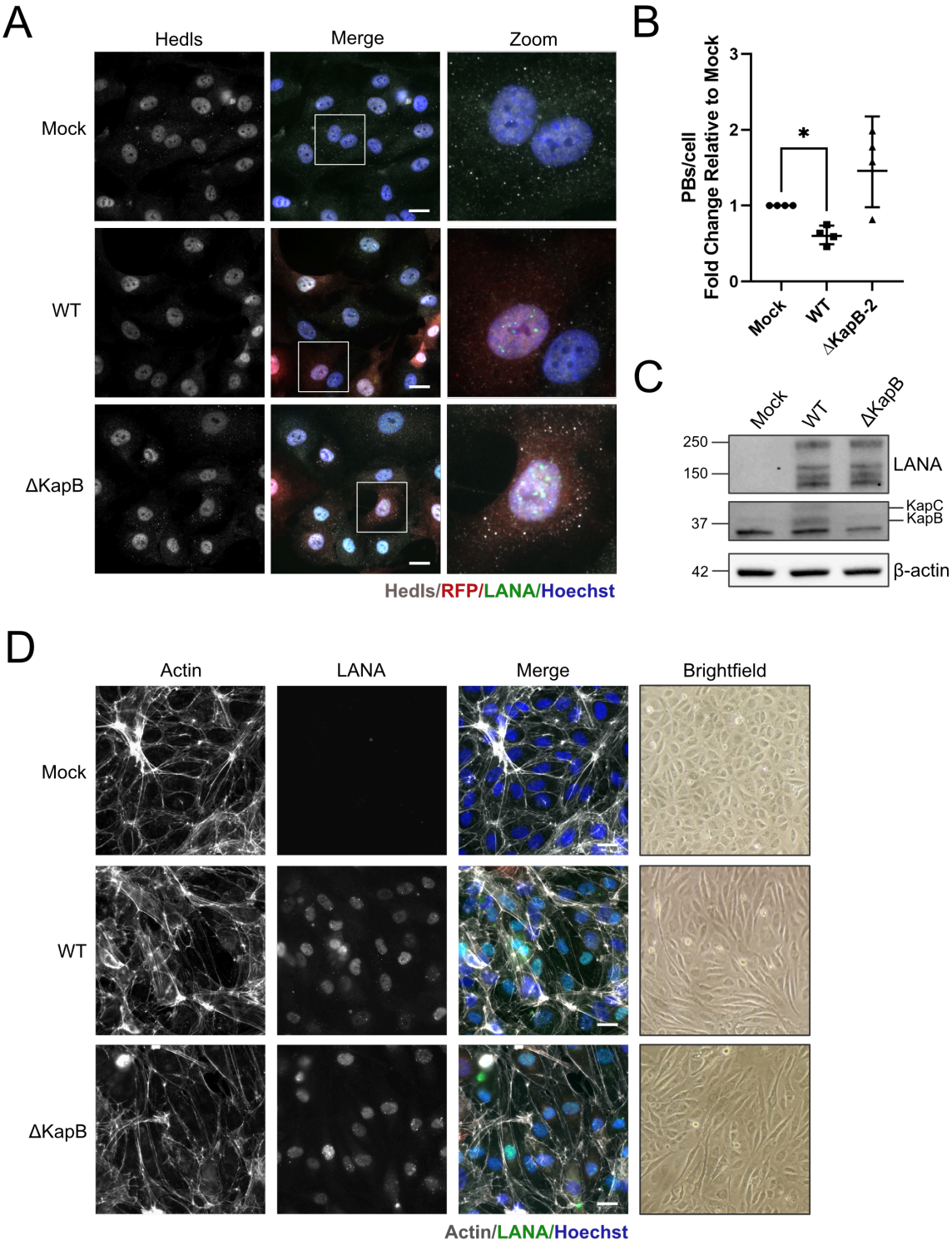
A
Hedls
Merge
Zoom
Mock
WT
ΔKapB
Hedls/RFP/LANA/Hoechst
B
PBs/cell
Fold Change Relative to Mock
3
2
1
0
*
Mock
WT
ΔKapB-2
C
Mock
WT
ΔKapB
250
150
LANA
37
KapC
KapB
42
β-actin
D
Actin
LANA
Merge
Brightfield
Mock
WT
ΔKapB
Actin/LANA/Hoechst